

AD-A098 649 TEXAS A AND M UNIV COLLEGE STATION DEPT OF ELECTRICAL--ETC F/G 7/1  
FEASIBILITY STUDY ON ADVANCED SOLID-STATE OXYGEN SENSORS. (U)  
DEC 80 M HAM F33615-78-0-0629

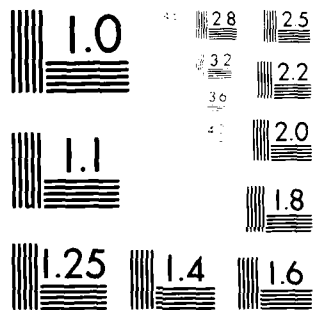
UNCLASSIFIED

SAM-TR-80-44

NL

1 of 1  
AD-A  
598 649

END  
DATE  
FILMED  
6-81  
DTIC



MICROCOPY RESOLUTION TEST CHART  
 NATIONAL BUREAU OF STANDARDS-1963-A

Report SAM-TR- 80-44

LEVEL *11*

*12*  
*BS*

## FEASIBILITY STUDY ON ADVANCED SOLID-STATE OXYGEN SENSORS

Mooyoung Ham, Ph. D.  
Department of Electrical Engineering  
Texas A&M University  
College Station, Texas 77843

DTIC  
ELECTRONIC  
S MAY 8 1981  
C

December 1980

Final Report for Period 29 February - 30 September 1980

Approved for public release; distribution unlimited.

Prepared for  
USAF SCHOOL OF AEROSPACE MEDICINE  
Aerospace Medical Division (AFSC)  
Brooks Air Force Base, Texas 78235



81 5 08 054

AD A098649

DIC FILE COPY

## NOTICES

This final report was submitted by the Department of Electrical Engineering, Texas A&M University, College Station, Texas 77843, under contract F33615-78-D-0629/0021, job order 7930-11-51, with the USAF School of Aerospace Medicine, Aerospace Medical Division, AFSC, Brooks Air Force Base, Texas. Dr. Kenneth Ikels (USAFSAM/VNL) was the Laboratory Project Scientist-in-Charge.


When U.S. Government drawings, specifications, or other data are used for any purpose other than a definitely related Government procurement operation, the Government thereby incurs no responsibility nor any obligation whatsoever; and the fact that the Government may have formulated, furnished, or in any way supplied the said drawings, specifications, or other data is not to be regarded by implication or otherwise, as in any manner licensing the holder or any other person or corporation, or conveying any rights or permission to manufacture, use, or sell any patented invention that may in any way be related thereto.

This report has been reviewed by the Office of Public Affairs (PA) and is releasable to the National Technical Information Service (NTIS). At NTIS, it will be available to the general public, including foreign nations.

This technical report has been reviewed and is approved for publication.

  
KENNETH G. IKELS, Ph.D.  
Project Scientist

  
RICHARD L. MILLER, Ph.D.  
Supervisor

  
ROY L. DEHART  
Colonel, USAF, MC  
Commander

UNCLASSIFIED

SECURITY CLASSIFICATION OF THIS PAGE (When Data Entered)

REPORT DOCUMENTATION PAGE		READ INSTRUCTIONS BEFORE COMPLETING FORM
1. REPORT NUMBER SAM-TR-80-44	2. GOVT ACCESSION NO. AD-A098649	3. RECIPIENT'S CATALOG NUMBER
4. TITLE (and Subtitle) FEASIBILITY STUDY ON ADVANCED SOLID-STATE OXYGEN SENSORS		5. TYPE OF REPORT & PERIOD COVERED Final Report- 29 Feb - 30 Sep 1980
7. AUTHOR(s) Mooyoung/Ham, Ph.D		6. PERFORMING ORG. REPORT NUMBER
9. PERFORMING ORGANIZATION NAME AND ADDRESS Department of Electrical Engineering Texas A&M University College Station, Texas 77843		8. CONTRACT OR GRANT NUMBER(s) F33615-78-D-0629/0021
11. CONTROLLING OFFICE NAME AND ADDRESS USAF School of Aerospace Medicine (VNL) Aerospace Medical Division (AFSC) Brooks Air Force Base, Texas 78235		10. PROGRAM ELEMENT, PROJECT, TASK AREA & WORK UNIT NUMBERS 62202F 7930-11-51
14. MONITORING AGENCY NAME & ADDRESS (if different from Controlling Office)		12. REPORT DATE December 1980
		13. NUMBER OF PAGES 45
		15. SECURITY CLASS. (of this report) Unclassified
16. DISTRIBUTION STATEMENT (of this Report)  Approved for public release; distribution unlimited.		15a. DECLASSIFICATION/DOWNGRADING SCHEDULE
17. DISTRIBUTION STATEMENT (of the abstract entered in Block 20, if different from Report)		
18. SUPPLEMENTARY NOTES		
19. KEY WORDS (Continue on reverse side if necessary and identify by block number)  Oxygen sensor, solid-state oxygen sensor		
20. ABSTRACT (Continue on reverse side if necessary and identify by block number)  This report comparatively reviews the three most widely known oxygen-sensing materials--stabilized $ZrO_2$ , $ZnO$ , and $TiO_2$ . The report also briefly describes gas-sensing MOS transistors and diodes that use Pd or Pt as a catalytic electrode material.		

DD FORM 1 JAN 73 1473

UNCLASSIFIED

SECURITY CLASSIFICATION OF THIS PAGE (When Data Entered)

## TABLE OF CONTENTS

	<u>Page</u>
INTRODUCTION . . . . .	3
REVIEW OF SOLID-STATE OXYGEN SENSORS . . . . .	4
Stabilized Zirconia Solid Electrolytes . . . . .	4
Zirconia Electrolyte Cell . . . . .	7
Zinc Oxide Semiconductor . . . . .	15
Rutile (Titanium Dioxide) Semiconductor . . . . .	30
Other Oxygen Gas Sensors . . . . .	35
REVIEW AND RECOMMENDATIONS . . . . .	37
REFERENCES . . . . .	40

### List of Illustrations

#### Figure

1	(a) Frenkel (interstitial) and Schottky (vacancy) models of lattice defects that can result in ionic conductivity. (b) Three classical mechanisms for ionic conductivity in crystalline solids (17)	5
2	The fluorite ( $\text{CaO-ZrO}_2$ ) structure	6
3	A typical galvanic cell using a zirconia oxygen ion electrolyte	8
4	The closed-loop concept of engine operation	10
5	Oxygen partial pressure vs. air/fuel ratio at $700^\circ\text{C}$	10
6	Schematic view of Lambda-sensor	11
7	Theoretical dependence of EMF of oxygen concentration cell with and without catalytically active electrode as a function of air/fuel ratio	12
8	Temperature dependence of electrical resistance of sensors with $\text{CaO-}$ and $\text{Y}_2\text{O}_3$ -stabilized ceramic	13
9	Schematic view of the protective layer used by Ichikawa et al.	14
10	Schematic illustration of zirconia exhaust sensor (cross-sectional view)	14
11	Experimental sensor voltage curve obtained using computer-controlled test facility	15
12	The wurtzite lattice of zinc oxide	16
13	Effect of chemisorption of electronegative molecules on surface on n-type semiconductor	19
14	Energy level diagram showing electron transfer over surface potential barrier	21
15	Electrical conductance of zinc oxide vs. increasing temperature for various partial pressures of oxygen	23
16	Photoconductivity sample holder and circuit arrangement for measuring photoresponse of $\text{ZnO}$ in nitrogen and oxygen environments	24

<u>Figure</u>		<u>Page</u>
17	Typical photoconductivity response of ZnO in oxygen (a) and nitrogen (b) environments. Horizontal-20 $\mu$ s/div., vertical-0.2 $\mu$ A/div., base line-0.5 div. from the top grid line . . . . .	25
18	Cross-sectional view of Wortman's sensor . . . . .	26
19	Resistance as a function of reciprocal temperature for three ZnO film thicknesses. Data taken at a constant cooling rate under 133 N/m <sup>2</sup> (1 Torr) oxygen pressure . . . . .	27
20	Resistance as a function of reciprocal temperature for 180-nm ZnO film at a constant cooling rate at a pressure of 133 N/m <sup>2</sup> (1 Torr) of the gases indicated . . . . .	28
21	Response time vs. temperature . . . . .	29
22	Unit cell of rutile (TiO <sub>2</sub> ). . . . .	31
23	Resistivity of TiO <sub>2</sub> ceramic as a function of partial oxygen pressure at several different temperatures . . . . .	33
24	Exploded view of construction of temperature-stabilized TiO <sub>2</sub> A/F sensor . . . . .	34
25	Basic principles of hydrogen-sensitive Pd (or Pt)-SiO <sub>2</sub> -Si structures . . . . .	36
26	A schematic diagram of the Pd-TiO <sub>2</sub> diode and the measuring cell . . . . .	37
27	The I-V curves of a Pd-TiO <sub>2</sub> diode in vacuum ( $2 \times 10^{-5}$ Torr) (a), and in oxygen atmosphere ( $1 \times 10^{-1}$ Torr) (b) . . . . .	38

#### List of Tables

<u>Table</u>		
1	Activation energies and preexponential terms for various stabilized ZrO <sub>2</sub> . . . . .	7
2	Requirements for Lambda-sensor and its maximum permissible operating condition limits . . . . .	11
3	Properties of ZnO . . . . .	17
4	Dependence of thermal activation energy on type of gas and pressure for 180-nm film . . . . .	26

Accession For	
NTIS GRA&I	<input checked="checked" type="checkbox"/>
DTIC TAB	<input type="checkbox"/>
Unannounced	<input type="checkbox"/>
Justification	
By	
Distribution/	
Availability	
Dist	
A	

## FEASIBILITY STUDY ON ADVANCED SOLID-STATE OXYGEN SENSORS

### INTRODUCTION

As part of an ongoing project for an advanced-oxygen-sensor feasibility study at the USAF School of Aerospace Medicine, a literature survey was conducted in the areas of solid-state thin-film oxygen sensors. This report is not an exhaustive compilation of all the pertinent references; however, it adequately covers the important and relevant developments of solid-state sensors that can meet most of the basic criteria for in-flight application:

- 1) low weight
- 2) small size
- 3) unaffected by ambient pressure change - 760-100 mm Hg
- 4) orientation insensitive
- 5) short response time - ~ few seconds
- 6) unaffected by motion and vibration
- 7) low power consumption
- 8) temperature insensitive - below 0 to 100°C
- 9) maintenance schedule - once/year
- 10) operable in less than 5 minutes
- 11) capable of withstanding up to 7 Gs.

Until the end of the 19th century, the only common methods of gas analysis were chemical methods which, in principle, consisted of removing one component of a gas mixture. Measurements of the change in temperature, pressure, and volume of the gas, allowed the quantity of the removed component to be detected (1). Approximately at the beginning of the 20th century, physical methods of gas analysis became more common. These methods include the use of physical principles of acoustic waves, thermal conductivity, dielectric susceptibility, magnetic dipole, mass spectrometry, and adsorption on metal oxide films.

In the last few years, rapid development has taken place in research on the surface effects of compound semiconductors and solid electrolytes on oxygen partial pressure. This development was partially due to newly recognized potential applications of solid-state sensors using today's well-developed integrated circuit technology. Among the many kinds of solid-state transducers (2), the five most widely known film oxygen sensors are  $\text{TiO}_2$ ,  $\text{Y}_2\text{O}_3\text{-ZrO}_2$ ,  $\text{CaO-ZrO}_2$ ,  $\text{ZrO}_2$ , and  $\text{ZnO}$  (3, 4, 5, 6-8, and 9-14, respectively).

The yttria- or calcia-stabilized zirconia film sensors, along with  $\text{ZrO}_2$  film, have been actively investigated by automobile industries and tested for reduction of automobile exhaust emission. These solid-state electrolyte sensors form part of a closed-loop system for control of the air-fuel ratio of the fuel mixture entering the engine. These kinds of sensors are primarily designed to be used as switching devices that indicate lean or rich content of oxygen in the exhaust gas by using the atmospheric pressure as a reference. This type of restriction will make their application to an aircraft difficult.



The practical application of titania sensors started appearing in the scientific literature in 1975 (15). Recently reported results on  $\text{TiO}_2$  film indicate its potential use as an oxygen sensor (3).

Among the sensors previously mentioned,  $\text{ZnO}$  film, which is an n-type semiconductor, has been most extensively studied and accepted as a good oxygen sensor. The zinc-oxide film seems to be the most promising for an aircraft application at this point. However, since the amount of technical information available in the literature about  $\text{TiO}_2$  (which is also a semiconductor) is much less than that for  $\text{ZnO}$ , ruling out the potential applicability of  $\text{TiO}_2$  sensors for the same purpose may be premature.

An interesting development has recently occurred in the areas of ion-sensitive MOS transistors and diodes. These devices use catalytic metals such as palladium (Pd) or platinum (Pt) as gate material for a transistor or as Schottky barrier for a diode. Even though these devices have been developed to detect hydrogen gas, they exhibit promising characteristics in oxygen ambient.

## REVIEW OF SOLID-STATE OXYGEN SENSORS

### Stabilized Zirconia Solid Electrolytes

In a perfect lattice, an atom would be located on every lattice site and ionic mobility would not occur. In real materials, however, defects exist--such as vacant lattice sites,<sup>1</sup> interstitial ions,<sup>2</sup> or interstitialcy ions<sup>3</sup>--which contribute to ionic conduction (Fig. 1). These defects are always present owing to composition or to thermal energy. Indeed, the existence of solid-compound electrolyte with practically pure ionic conductivity has been known for some time, and Rickert (16) compiled some of the earlier work published in this field.

The solid solutions of calcia ( $\text{CaO}$ ), yttria ( $\text{Y}_2\text{O}_3$ ), or other rare-earth oxides in zirconia ( $\text{ZrO}_2$ ) are known to change its crystal structure (18-23). Within certain concentration ranges, such solutions crystallize in a cubic phase which is stable in the desired temperature range of 300-900°C, and show approximately pure oxygen ion conductivity. Figure 2 shows the crystal structure of calcia-stabilized zirconia (19). The ion conductivity results from the substitution of tetravalent ions in the crystal lattice by cation of lower

---

<sup>1</sup>Vacant lattice sites (vacancies) - These are missing ions, compared to the perfect lattice.

<sup>2</sup>Interstitial ions - These are excess ions, compared to the perfect lattice.

<sup>3</sup>Interstitialcy ions - These ions hop to interstitial sites, and interstitial ions fill the remaining vacancies.

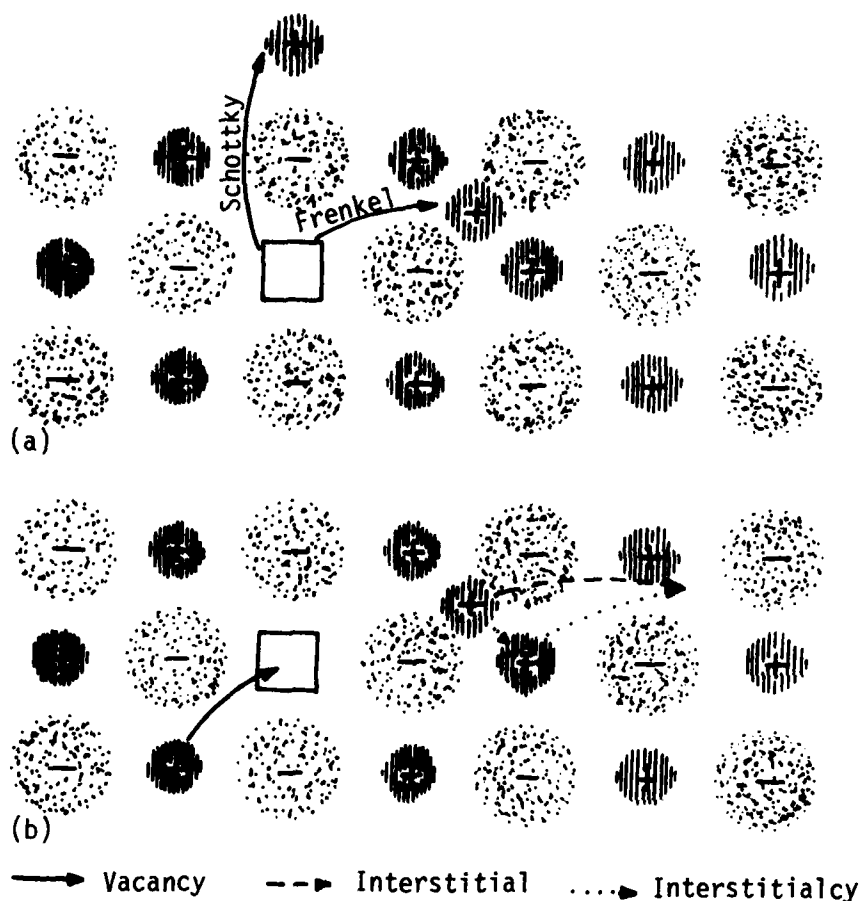


Figure 1. (a) Frenkel (interstitial) and Schottky (vacancy) models of lattice defects that can result in ionic conductivity. (b) Three classical mechanisms for ionic conductivity in crystalline solids (17).

valence, such as  $\text{Ca}^{+}$  or  $\text{Y}^{3+}$ . For reasons of electroneutrality, oxygen ion vacancies are created by the nonoccupancy of oxygen lattice sites. The transport of oxygen ions can take place via these vacancies. The value of the electrical conductivity is mainly determined by the nature of the stabilizer cation, the stabilizer concentration, and the temperature.

The electronic conductivity of stabilized zirconia is practically zero (16, 19). Hence, the ionic transference number,  $t$ , for oxygen ions, defined as the ratio of ionic conductivity to the total conductivity which may include electron and holes, is essentially unity:

$$t_{\text{ion}} = \sigma_{\text{ion}} / \sigma_{\text{total}} \approx 1 \quad (1)$$

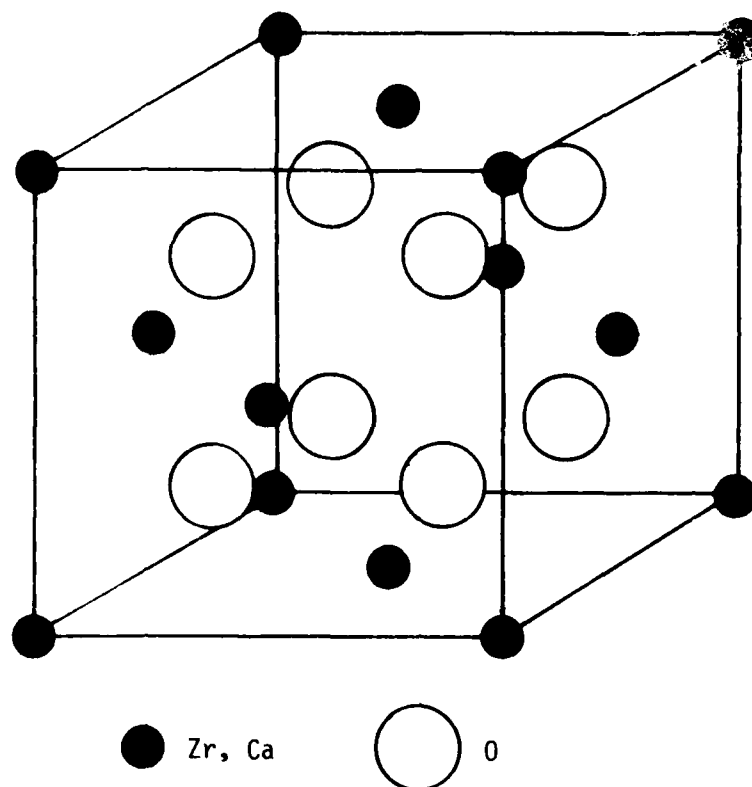


Figure 2. The fluorite ( $\text{CaO-ZrO}_2$ ) structure.

It is this feature of solid cubic zirconia which makes it of interest as an oxygen ion electrolyte. This point will be reemphasized at the end of the next section.

One limitation of zirconia as an oxygen ion electrolyte is that the ionic conductivity does not become significant until the zirconia material is heated to temperatures exceeding approximately  $300^\circ\text{C}$  (23). The ionic conductivity of zirconia is independent of oxygen partial pressure and varies exponentially with temperature according to the Arrhenius relation

$$\sigma = A \cdot \exp(-E_a/kT) \quad (2)$$

where  $A$  = a preexponential term

$E_a$  = the activation energy

$k$  = the Boltzmann constant

$T$  = the absolute temperature (19).

The values of  $E_a$  and  $A$  vary according to the composition of the stabilized zirconia. Table 1 shows the typical values of  $E_a$  and  $A$  for several zirconia compositions (24).

TABLE 1. ACTIVATION ENERGIES AND PREEXPONENTIAL TERMS FOR VARIOUS STABILIZED  $ZrO_2$

Stabilizer content (mole %)	$E_a$ (in eV)	$A$ (in $\Omega^{-1}$ )
15 CaO	1.260	1500.0
8 $Y_2O_3$	0.738	86.2
8 $Yb_2O_3$	0.751	83.4
10 $Sc_2O_3$	0.645	90.4
6 $Sm_2O_3$	0.869	97.2

### Zirconia Electrolyte Cell

A typical galvanic cell using a zirconia solid electrolyte is shown in Figure 3 (18, 23, 25-28). A thin plate of zirconia ceramic separates two gas atmospheres having oxygen partial pressures  $p_{O_2}^1$  and  $p_{O_2}^2$ . Each surface

of the zirconia plate is coated with a porous electrode material, such as Pt or Pd, which promotes the electrochemical reaction:



where  $e^-$  represents an electron and  $O^-$  represents an oxygen ion. The oxygen partial pressure can be related to the chemical potential by the relation (29, 30)

$$\mu_i = \mu_0 + (RT/2) \ln p_{O_2}^i \quad (4)$$

where  $i = 1$  and  $2$  denotes two electrodes,  $R$  is the gas constant ( $8.313435$  J/mole), and  $T$  is the absolute temperature.

The galvanic potential can be calculated now by the equation

$$\phi = - \frac{1}{ZF} \int_{\mu_1}^{\mu_2} t_{ion} d\mu \quad (5)$$

where  $Z$  is the valence of the oxygen ion which is  $2$ ,  $F$  is the Faraday constant ( $9.65 \times 10^4$  C/mole), and  $t_{ion}$  is the ionic transference number which is nearly  $1$  (19). From Eqs. 4 and 5, one can obtain

$$\begin{aligned} \phi &= - \left( \frac{RT}{2ZF} \right) \int_{p_{O_2}^1}^{p_{O_2}^2} (t_{ion}/p_{O_2}) dp_{O_2} \\ \phi &\approx - \left( \frac{RT}{4F} \right) \ln(p_{O_2}^1/p_{O_2}^2) \end{aligned} \quad (6)$$

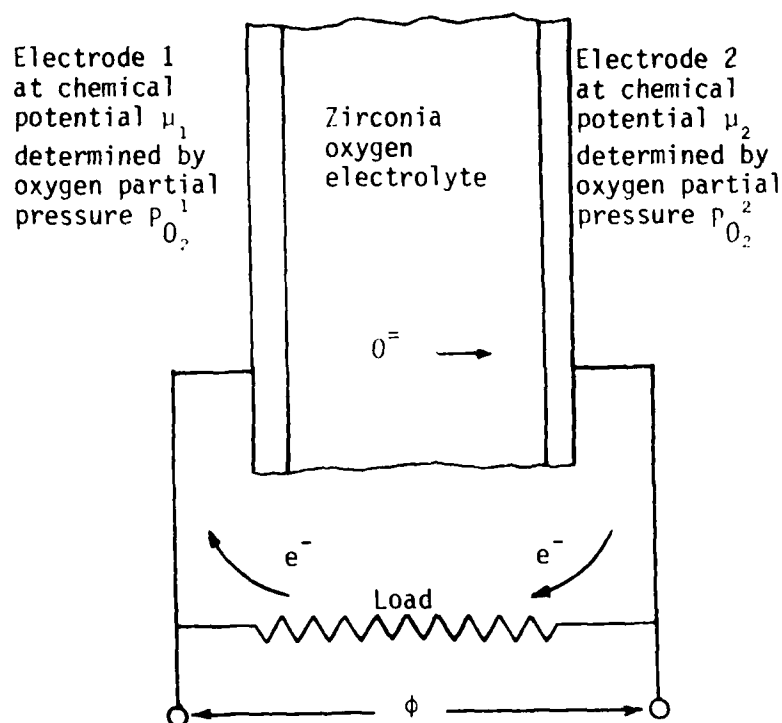


Figure 3. A typical galvanic cell using a zirconia oxygen ion electrolyte.

which is known as a form of the Nernst equation. Note: Eq. 6 is valid only if the contributions of electrons and holes to the total conductivity are negligible (18).

If the conductivity of a stabilized zirconia cell is, practically, not a function of the oxygen pressure, how can the cell be used to measure oxygen partial pressure? Even though the conductivity is only a function of temperature, the galvanic potential developed across the cell is a function of the oxygen pressure. It is then ultimately desirable to have a constant internal conductivity as the oxygen partial pressure varies. This very characteristic makes the zirconia cell a potential oxygen sensor.

**Applications**--Over the past years, many systems for achieving low exhaust-emission levels in automobile engines have been investigated (31). The various systems permit more accurate fuel metering, better preparation and distribution of the mixture, and improved combustion and treatment of the exhaust gases in catalytic converters. The  $ZrO_2$ -type oxygen sensors have been experimented with most extensively (4, 6-8, 23, 32-35). This section includes descriptions of the several sensors reported in the last few years.

It is very interesting to see that, recently, the automobile industry has begun producing cars (1981 models) with exhaust-gas sensors even though a precise relation of the exhaust gas composition to air-fuel (A/F) ratio was well investigated by D'Alleva et al. in 1936 (36). A zirconia A/F ratio sensor, inserted into the exhaust manifold of the tailpipe, senses the large change in the oxygen partial pressure,  $P_{O_2}$ , at the stoichiometric A/F ratio (Fig. 4). The oxygen pressure is shown as a function of A/F ratio in Figure 5. Because of the large and sharp change in the oxygen partial pressure at the stoichiometric A/F ratio, the zirconia sensor output exhibits a stepwise change at this air-fuel ratio, which is used as a feedback signal to control injection system (3).

Hamann (4), Ichikawa (32), and Dueker (23) reported characteristics of zirconia sensors that had a similar shape in their mechanical construction. Among these reports, Dueker's was the most thorough. Figures 6 to 8 show the construction and various characteristics of the Bosch Lambda-sensor, and Table 2 shows the most important requirements of the sensor and its limits of operating conditions.

Figure 6 shows details of the calcia-stabilized zirconia oxygen sensor. As explained earlier, oxygen ions move through this solid electrolyte and develop an electromotive force across the inner and outer electrodes according to the Nernst equation. Platinum is used as electrode material to insure catalytic reaction at the interface between the exhaust gas and the electrolyte. The Pt surface is made porous so that the gas can have easy contact with the zirconia cell. Ichikawa (32) designed a similar sensor and used an ingenious method to build a protective layer on the porous outer Pt electrode (Fig. 9). The protective layer is necessary because of hot exhaust gas (Table 2). By bonding zirconia particles ( $0.5\text{--}5\text{ }\mu\text{m}$ ) onto the porous electrode, he was able to produce pores ( $1\text{--}2\text{ }\mu\text{m}$ ) within the protective layer. Powders of borosilicate glass were used as the adhesive.

The importance of the catalytic metal is shown in Figure 7. The theoretical curve b is reached only when the catalytic activity of the exhaust electrode suffices to establish complete equilibrium, the electrode exhibits pure oxygen ion conductivity, and the voltage is measured at practically zero current.

Figure 8 shows the Arrhenius relation (Eq. 2) of the electrical resistance of sensors with CaO- and  $Y_2O_3$ -stabilized ceramics. Data given in Figure 8 is about an order of magnitude less than that reported by Dixon (37). The apparent difference is coming from different fabrication processes that they used.

The zirconia sensor designed by Fleming (6) is shown in Figure 10; and a typical response of the sensor, in Figure 11. As indicated by Figure 5, a sharp and large change in the voltage output occurs at the point of A/F stoichiometry. The voltage step resulting at  $A/F = 1$  serves as the control signal in the closed-loop system.

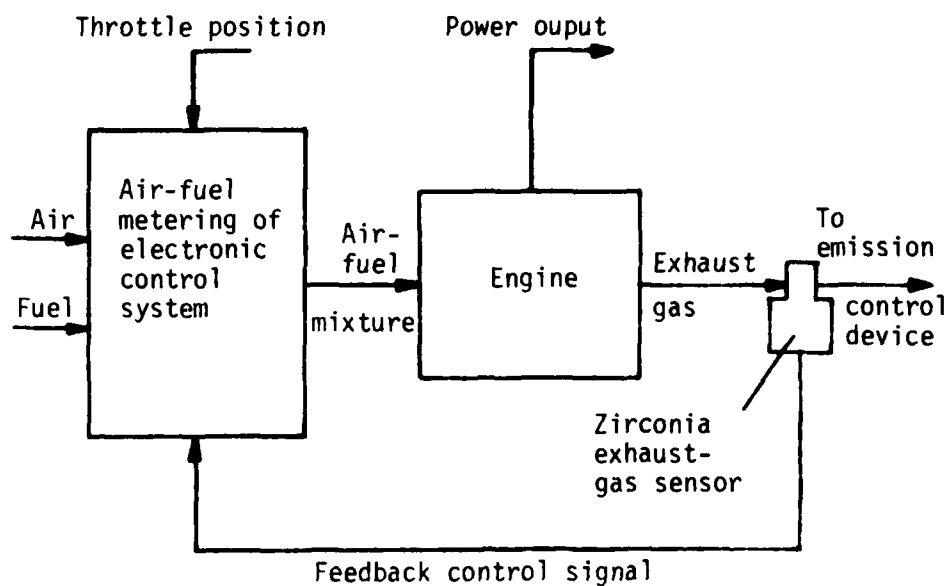


Figure 4. The closed-loop concept of engine operation.

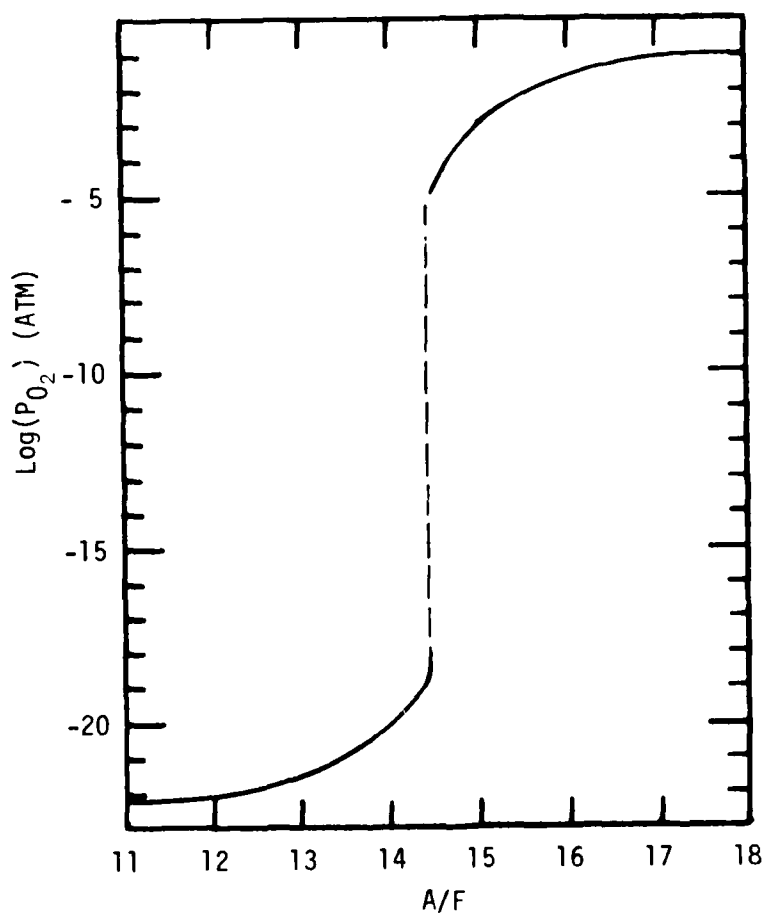


Figure 5. Oxygen partial pressure vs. air/fuel ratio at 700°C.

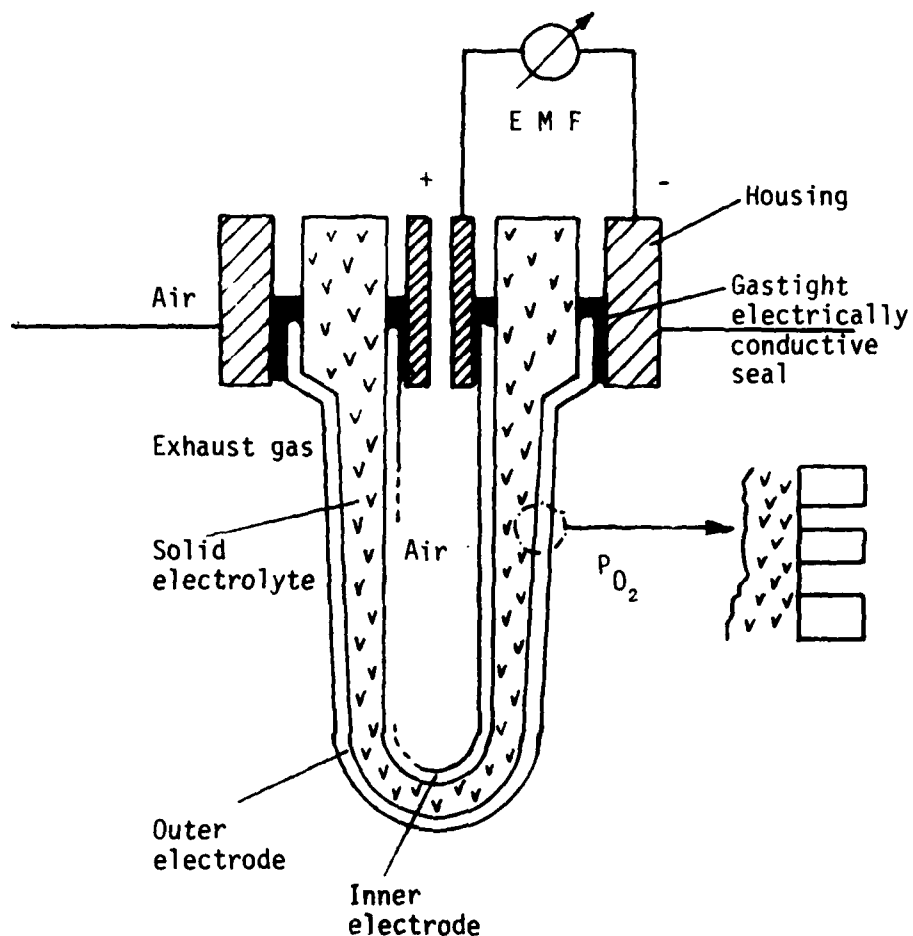


Figure 6. Schematic view of Lambda-sensor.

TABLE 2. REQUIREMENTS FOR LAMBDA-SENSOR AND ITS MAXIMUM PERMISSIBLE OPERATING CONDITION LIMITS (23)

Requirements

Height of voltage signal:	$\geq 500\text{-}600\text{ mV}$ , measured between $A/F = 0.95$ and $A/F = 1.05$
Response time:	$\leq 50\text{ ms}$ at $700^\circ\text{C}$
Starting temperature:	$300\text{-}400^\circ\text{C}$
Internal resistance:	$\leq 10^5\ \Omega$ (at $400^\circ\text{C}$ )
Lifetime:	$\geq 15,000$ miles

Operating condition limits

Temperature at ceramic tip: max.  $900^\circ\text{C}$   
 Thermal shocks at ceramic tip: max.  $20^\circ\text{C/s}$   
 Vibration acceleration of ceramic body: max. 60 Gs.



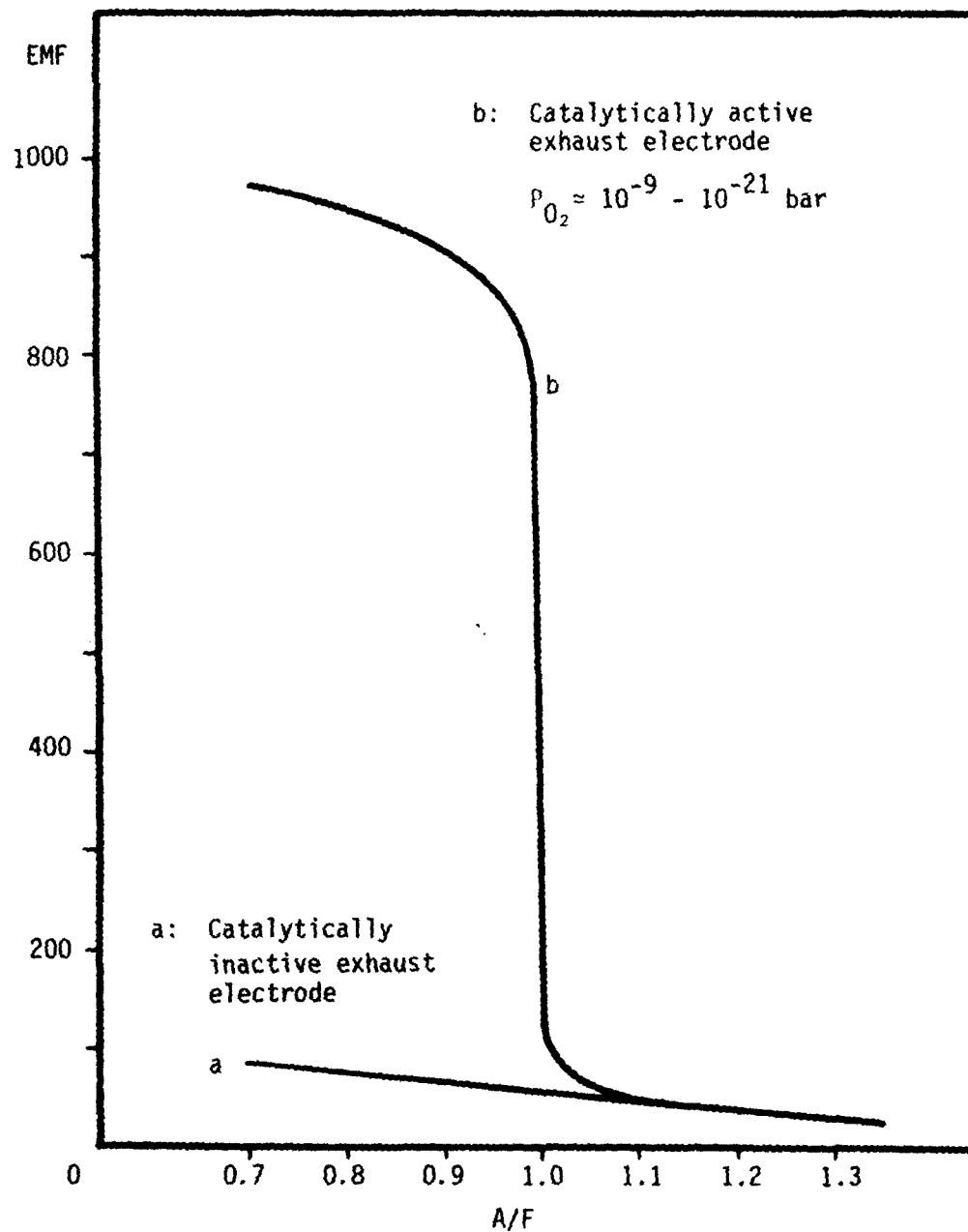


Figure 7. Theoretical dependence of EMF of oxygen concentration cell with and without catalytically active electrode as a function of air/fuel ratio.

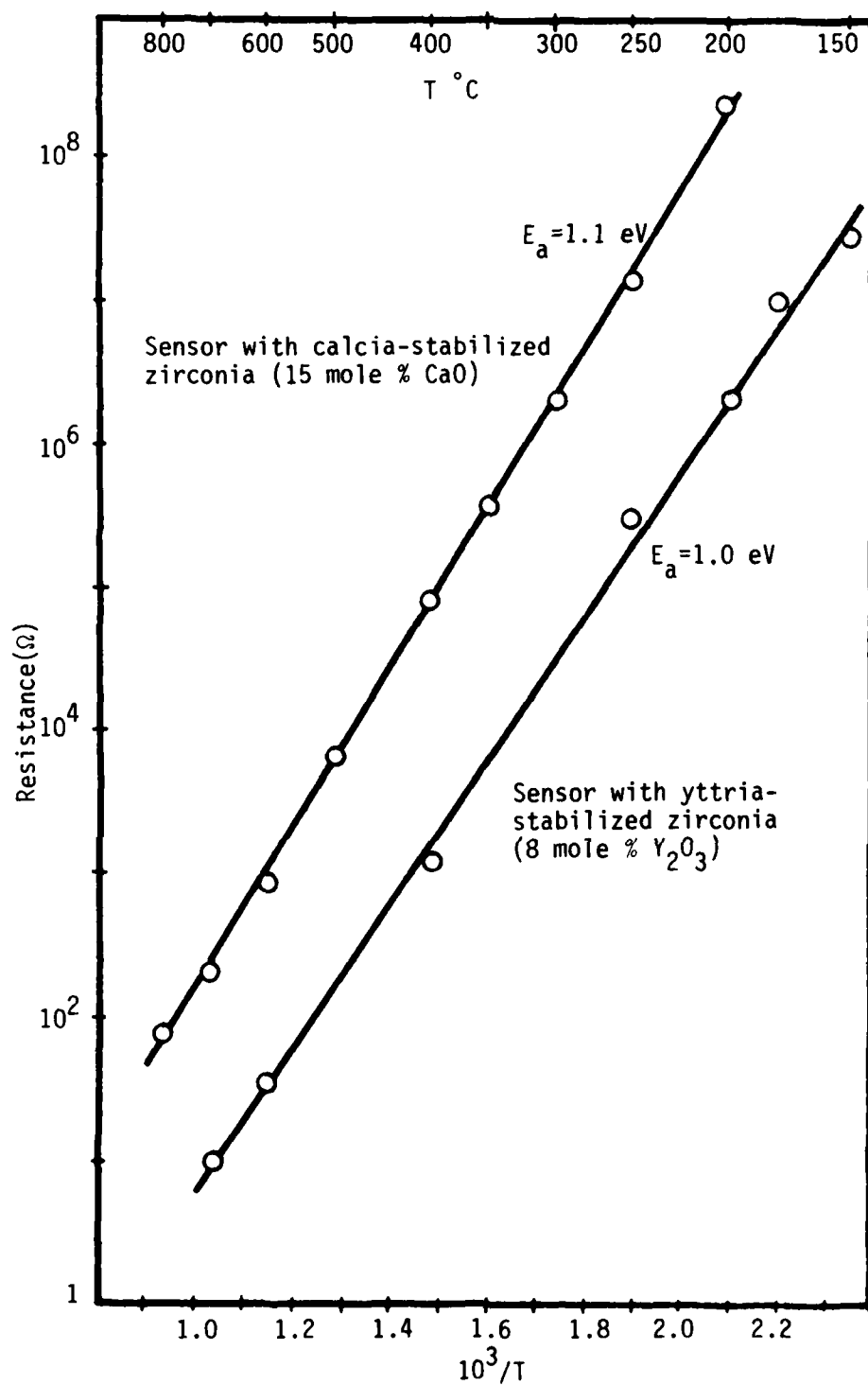
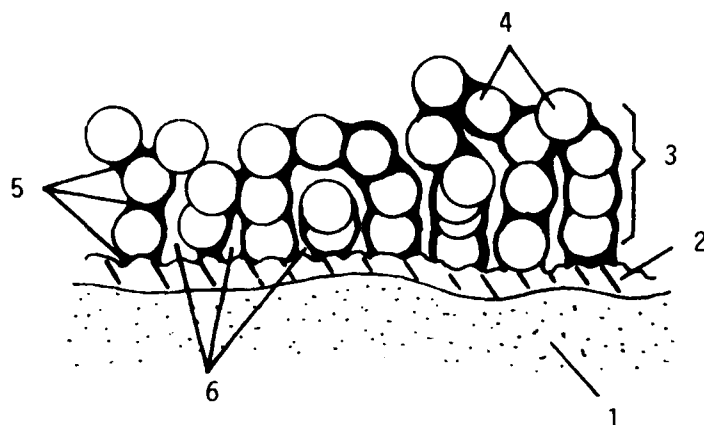


Figure 8. Temperature dependence of electrical resistance of sensors with  $\text{CaO}$ - and  $\text{Y}_2\text{O}_3$ -stabilized ceramic.



- 1 - Zirconia layer
- 2 - Porous platinum layer
- 3 - Protective layer
- 4 - Zirconia particles
- 5 - Borosilicate adhesive
- 6 - Pores for oxygen passage

Figure 9. Schematic view of the protective layer used by Ichikawa et al.

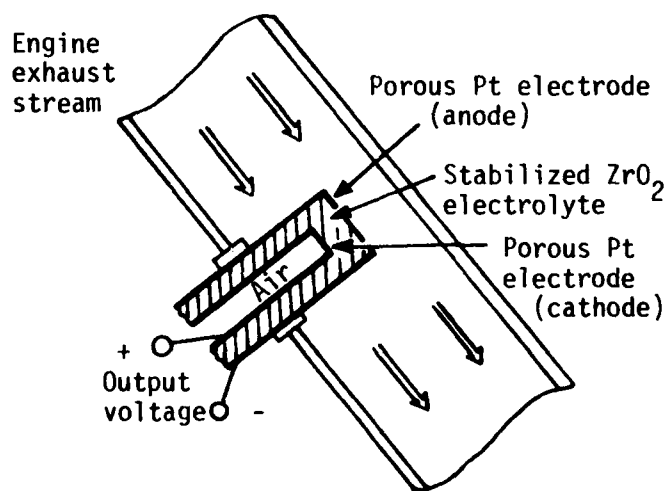


Figure 10. Schematic illustration of zirconia exhaust sensor (cross-sectional view).

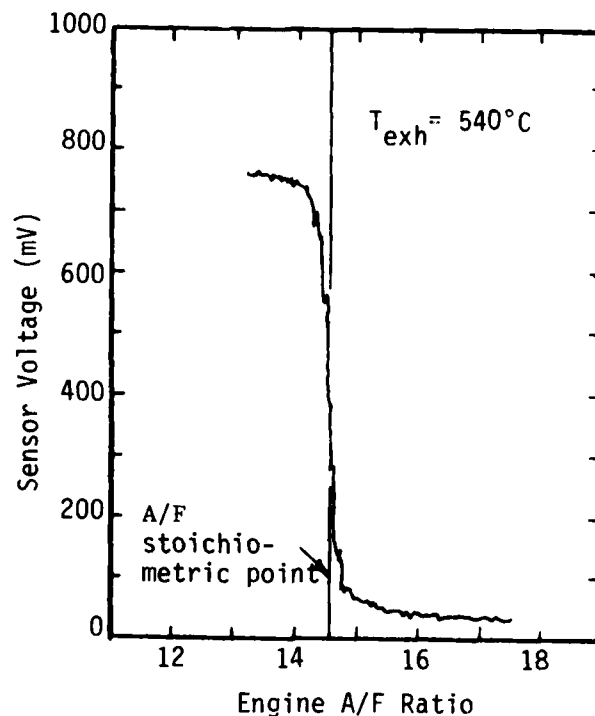


Figure 11. Experimental sensor voltage curve obtained using computer-controlled test facility.

Summary--Physical principles of stabilized-zirconia oxygen sensors are reviewed, with some illustrations of actual application in the automobile exhaust system. This type of solid-electrolyte sensor requires a reference pressure, which is necessary in using the Nernst equation (Eq. 6), and needs to be heated in the range of 400 ~ 900°C. In the automobile application, the atmospheric pressure is used as the reference. The sensor fabrication process causes the sensor's response to vary in a wide range.

#### Zinc Oxide Semiconductor

Zinc oxide, ZnO, occurs in nature as the mineral zincite. It is produced in large quantities in the smelting of zinc ores, and can be prepared in pure form by burning zinc in air. The material has played only a subordinate role as a semiconductor, photoconductor, and phosphor. Occasionally, it has been used as a phosphor because of its rapid decay time.

ZnO crystallizes in the hexagonal wurtzite lattice, in which the oxygen ions are arranged in closest hexagonal packing and the zinc ions occupy half of the tetrahedral interstitial positions and have the same relative arrangement as the oxygen ions (Fig. 12) (38). Actually the environment of each ion does not have exact tetrahedral symmetry. Instead, the spacing between nearest neighbors in the direction of the hexagonal, or c axis, is somewhat smaller than for the other three neighbors.

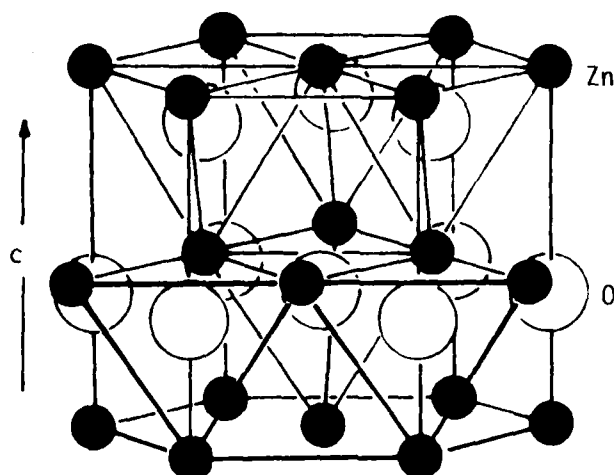


Figure 12. The wurtzite lattice of zinc oxide.

The most important mechanical and thermal properties of zinc oxide are listed in Table 3. Most of the values differ for specimens of different origin. The differences in the lattice constant are on the order of one percent, whereas the differences in density are on the order of ten percent. In cases of structure-sensitive properties, such as the magnetic susceptibility and the dielectric constant, only the order of magnitude is sure (38).

Electrically, ZnO film, whether it is a single crystal or a polycrystal, is an n-type semiconductor whose band gap and work function are 3.2 eV and 4.8 eV respectively (40, 41).

Chemisorption Model--To avoid confusion, definitions of a few terms are given below. Adsorption of gas molecules at the surface of a solid is customarily divided into two categories: a) physical adsorption, or physisorption, and b) chemisorption. Morrison, Tompkins, and Adamson (42-44) give excellent discussions on the above subjects, and Flood (45) compiled several thousand references in the areas of solid-gas interfaces.

a) Physisorption is characterized by long-range bonding originating from the van der Waals polarization interactions. Noble-gas adsorption on solid surfaces may be regarded as an example of physical adsorption. Physisorption is unlikely to affect the space-charge region of the surface of a semiconductor.

b) Chemisorption is characterized by strong, short-range chemical bonding accompanied by the liberation of large quantities of heat. Oxidation is a typical example of adsorption of this type. Chemisorbed species are often charged, producing or changing space-charge layers at the semiconductor surface. It is with such a process that chemisorbed species derive part or most of their binding energy from charge exchange with the semiconductor adsorbent.

TABLE 3. PROPERTIES OF ZnO (39)

Lattice	Hexagonal, wurtzite (B4-type)																				
Lattice constant	a = 3.24 Å, c = 5.19 Å, c/a = 1.60																				
Distance of neighboring Zn <sup>++</sup> - and O <sup>--</sup> -ions	In direction of the c axis d = 1.96 Å, of the three remaining neighbors d = $\sqrt{a^2/3 + c^2(u - 1/2)^2}$ = 1.98 Å (u = 0.378 instead of 0.375) for ideal tetrahedral arrangements																				
Molecular weight	Zn: 65.38; O: 16.00; ZnO: 81.38																				
Ionic radius for tetrahedral coordination	Zn <sub>neutral</sub> : 1.31 Å, O <sub>neutral</sub> : 0.66 Å, for covalent binding; Zn <sup>++</sup> : 0.70 Å, O <sup>--</sup> : 1.32 Å for ionic binding; Zn <sup>++</sup> : 0.78 Å, O <sup>--</sup> : 1.24 Å for ionic binding																				
Density	X-ray density 5.62-5.78 g/cm <sup>3</sup> , corresponding to 4.21 x 10 <sup>22</sup> ZnO-molecule/cm <sup>3</sup> , pycnometric: maxim 5.84 g/cm <sup>3</sup> , active ZnO:<5 g/cm <sup>3</sup>																				
Specific surface	Maximal larger than 80 m <sup>2</sup> /g for active ZnO																				
Enthalpy of formation	Zn (solid) + 1/2 O <sub>2</sub> (gas) → ZnO (solid): -83.17 kcal/mole corresponding to -3.61 eV/ZnO-molecules in lattice																				
Lattice energy	965 kcal/mole (from the Born-Haber cycle)																				
Specific heat	<table><tr><td>°K</td><td>20</td><td>30</td><td>50</td><td>100</td><td>150</td><td>209</td><td>300</td><td>500</td><td>900</td></tr><tr><td>cal/mole deg</td><td>0.17</td><td>0.60</td><td>1.98</td><td>4.24</td><td>6.22</td><td>7.20</td><td>9.66</td><td>11.2</td><td>12.3</td></tr></table>	°K	20	30	50	100	150	209	300	500	900	cal/mole deg	0.17	0.60	1.98	4.24	6.22	7.20	9.66	11.2	12.3
°K	20	30	50	100	150	209	300	500	900												
cal/mole deg	0.17	0.60	1.98	4.24	6.22	7.20	9.66	11.2	12.3												
Vapor pressure	12 Torr at 1500°C, 1 Torr at 1400°C, sublimation in high vacuum is appreciable at 1000°C																				
Melting point	≈ 2000°C only at high pressures																				
Dielectric constant	Values in literature for powder and sintered specimens between 10 and 36. Single crystals (2.4 x 10 <sup>10</sup> Hz): ε <sub>r</sub> = 8.5																				
Magnetic susceptibility	<table><tr><td>Temperature °K</td><td>273</td><td>196</td><td>83</td></tr><tr><td>ZnO (active)</td><td>-0.31</td><td>-0.20</td><td>+0.62</td></tr><tr><td>ZnO (tempered)</td><td>-0.26</td><td>-0.25</td><td>-0.25</td></tr></table> x 10 <sup>-6</sup>	Temperature °K	273	196	83	ZnO (active)	-0.31	-0.20	+0.62	ZnO (tempered)	-0.26	-0.25	-0.25								
Temperature °K	273	196	83																		
ZnO (active)	-0.31	-0.20	+0.62																		
ZnO (tempered)	-0.26	-0.25	-0.25																		

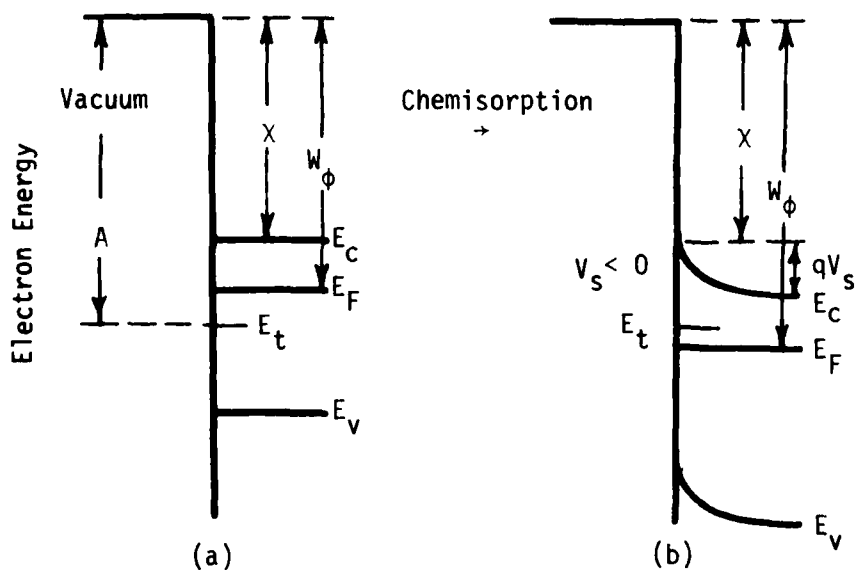
Consider a single electronegative molecule, such as oxygen, approaching the ZnO surface. If its electron affinity ( $A$ ) is larger than the semiconductor work function  $W\phi$ , the molecule will tend to pick up an electron from the semiconductor and thereby become chemisorbed at the surface. The difference between the electron affinity and the work function determines the position of the acceptor level,  $E_t$ , of the oxygen molecule. With further adsorption, the surface becomes more negatively charged while a positive space charge forms below it. In this process, the energy band at the surface bends upward and the work function increases until, at equilibrium, the Fermi levels of the semiconductor and the adsorbate are aligned. As the adsorption proceeds, the surface conductivity will be decreased due to the reduction of free electron concentration near the surface. The process is illustrated in Figure 13.

The rate of electron capture by the adsorbate equals, in equilibrium, the rate of electron release back to the conduction band of the semiconductor. The formation of a barrier ( $qV_s$ ) at the semiconductor surface is thus seen to affect both the equilibrium amount chemisorbed and the rate of chemisorption (41, 46, 47).

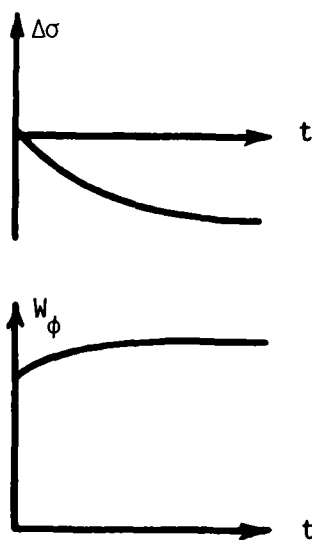
The adsorption process probably occurs in two stages. The first, and usually the faster, is physical adsorption. The slower, rate-limiting process is the charge exchange between the semiconductor and physisorbed molecule. Each physisorbed molecule converts into a chemisorbed one upon electron transfer to or from the semiconductor. The chemisorption bonds need not be completely ionic. An adsorbed molecule may be strongly bound to the surface in the neutral form by covalent-type bonding as the "weak" form of chemisorption. If, in addition, charge exchange with the semiconductor can take place, the bond involved would be strengthened and the strong form of chemisorption obtained (48).

As to the surface states, their presence can affect the adsorption process. For example, band bending usually occurs before chemisorption starts. More importantly, the adsorbate may change the surface-state structure by shifting the energy levels of the states and changing their density (46).

Although the chemisorption model just discussed is an over-simplification of the actual situation, it well illustrates the fundamental processes involved, such as charge transfer and the formation of a potential barrier.



(a,b)



$X$ : the electron affinity of the semiconductor

$E_C$ : the conduction band of the semiconductor

$E_F$ : the Fermi level of the semiconductor

$E_V$ : the valence band of the semiconductor

$\Delta\sigma$ : change in the surface conductivity of the semiconductor

Figure 13. Effect of chemisorption of electronegative molecules on surface of n-type semiconductor.



Evaluation of the Rate of Electron Transfer as a Function of Oxygen Pressure--The rate of oxygen-induced electron transfer between the bulk and the surface can be determined from the measured contact potential ( $V_C$ ) transient. For a depleted surface layer, as shown in Figure 14,  $dV_S$  can be related to the change in the density of net negative space charges at the surface as

$$dV_S = -\alpha(|V_S| - kT/q)^{1/2} dn_t \quad (7)$$

where  $n_t$  = density of electrons trapped at the surface  
 $\alpha = (2q/\epsilon_r \epsilon_0 n_b)^{1/2}$   
 $\epsilon_r$  = dielectric constant  
 $\epsilon_0$  = permittivity of free space  
 $n_b$  = bulk electron density  
 $q$  = absolute value of electronic charge (41).

Then, assuming  $dV_C \approx dV_S$ , which is justified in reference 41, the rate of electron transfer from the bulk into the oxygen-induced surface states becomes

$$R_{ct} = dn_t/dt = (dn_t/dV_S) (dV_C/dt) \quad (8)$$

Now  $R_{ct}$  can be determined from the measured rate of changes in contact potential difference  $dV_C/dt$ , since  $dn_t/dV_S$  can be obtained from Eq. 7. Thus the rate equation becomes

$$R_{ct} = \{-1/[\alpha(|V_S| - kT/q)^{1/2}]\} dV_C/dt \quad (9)$$

In semiconductors, the space charge region generally extends  $10^{-5}$  to  $10^{-4}$  cm beneath the surface. This distance is usually a sizable fraction of the sample thickness, so the contribution of surface conductance to the overall sample conductance is significant. Thus the measurement of conductance parallel to the surface, associated with the free carriers in the space-charge layer, can be related to  $R_{ct}$ .

For ZnO film, since it is n-type, the surface conductivity change is given by

$$\Delta\sigma = q\mu_n \Delta N \quad (10)$$

where  $\mu_n$  is the electron mobility, and  $\Delta N$  is the change in the number of electrons in the space-charge layer with respect to their number of flat bands ( $V_S = 0$ ). From the definition of  $n_t$ , one can see that<sup>4</sup>

<sup>4</sup>Although the authors of references 41 and 46 used piezoelectric modulation and field effect methods, respectively, to measure  $V_S$  as a function of time, it would be simpler to use Eqs. 10 and 11 because  $d\sigma/dt$  and  $dV_C/dt$  are both measurable quantities.

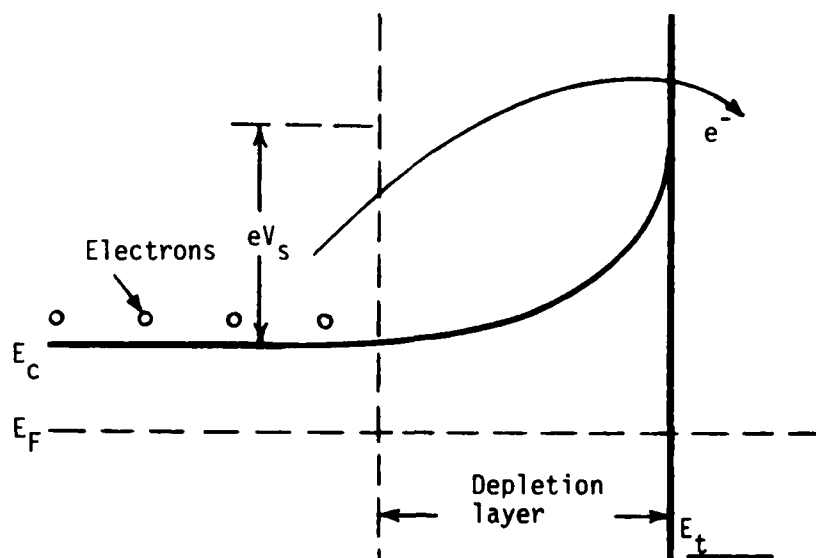


Figure 14. Energy level diagram showing electron transfer over surface potential barrier.

$$R_{ct} = dn_t/dt = -dN/dt = -(q\mu_n)^{-1}(d\sigma/dt) \quad (11)$$

As to the effect of the oxygen pressure ( $p_{O_2}$ ) to  $R_{ct}$ , there is no doubt that  $R_{ct} \propto p_{O_2}$  since  $dV_C/dt$  is. The latest and most comprehensive theoretical expression for  $R_{ct}$  reported so far is

$$R_{ct} = CA_n v_T n_b \exp[(qV_s + Q)/kT] \cdot \exp(-E_a/kT) \cdot p_{O_2} \quad (12)$$

where  $C$  = constant

$A_n$  = electron-capture cross section for chemisorption  
 $\approx 10^{-28} \sim 10^{-22} \text{ cm}^2$

$v_T$  = thermal velocity of conduction electrons

$Q$  = heat adsorption  $\approx 0.1 - 0.5 \text{ eV}$

$V_s = 0.05 \text{ V}$

$E_a$  = thermal activation energy  $\approx 0.25-0.72 \text{ eV}$  (41, 46).

As one can see from Eq. 12, the activation energy represents a most significant rate-limiting factor because of the negative sign attached to it.

Applications--Even though the property of zinc oxide film for its selective response to oxygen has been known for some time, the knowledge compiled

through basic researches over the last several decades<sup>5</sup> has not really been applied for making a good working solid-state oxygen sensor.

Royal et al. (49) and Wortman et al. (50) reported the most comprehensive experimental data about ZnO as an oxygen sensor in 1968 and 1972, respectively. They designed a ZnO-film oxygen sensor that measured the resistance (R) of the film as a function of the oxygen partial pressure. Their theoretical basis was Eq. 12. Since

$$R_{ct} \propto (-d\sigma/dt) \propto (-1/R), \text{ one can obtain that}^6$$

$$R = R_0 \cdot \exp(E_a/kT) \quad (13)$$

where  $R_0$  contains all of the physical constants and parameters discussed in Eq. 12. They have indeed shown empirically the validity of Eq. 13.

Royal (49) prepared the sensor film by oxidizing zinc film in oxygen at elevated temperatures. The film was deposited on  $Al_2O_3$  substrates by using standard vacuum evaporation techniques. Figure 15 shows the electrical conductance of zinc oxide film as a function of temperature. At a constant temperature, the film conductance is a strong function of the oxygen partial pressure. For example, at 700°K a change from 25%  $O_2$  - 75%  $N_2$  mixture to 100%  $O_2$  - 0%  $N_2$  results in a factor-of-three decrease in the film conductance. This type of data will be helpful in determining an optimum operating temperature of a sensor.

In addition to testing the zinc oxide films at elevated temperatures by observing the electrical conductivity, Royal (49) also measured the photoconductivity of the film by using a xenon flash lamp at a rate of ten flashes per second. The sample holder and circuit shown in Figure 16 were used to monitor the photocurrent, and Figure 17 shows the time response of the signal. Two significant advantages of observing the photoconductivity at room temperature rather than the electrical conductivity at an elevated temperature are the elimination of (1) the power required for the heater and (2) the need to provide reliable high-temperature electrical contacts to the sensing film (49). More detailed experimental data with theoretical analysis have been reported by others (51-54).

Matthews and Kohnke (55) and Royal (49) reported their unsuccessful attempts to produce stable zinc-doped thin oxide that would exhibit much shorter response time than that of pure zinc oxide at typically 270°C. The stability

---

<sup>5</sup>Reference 40, which is a review paper, cited 165 references. It is the most comprehensive publication ever done about ZnO film.

<sup>6</sup>Because the integration of Eq. 12 is quite involved,  $(d\sigma/dt)$  is used here rather than  $\int d\sigma$  and will be proportional to  $(1/R)$ .

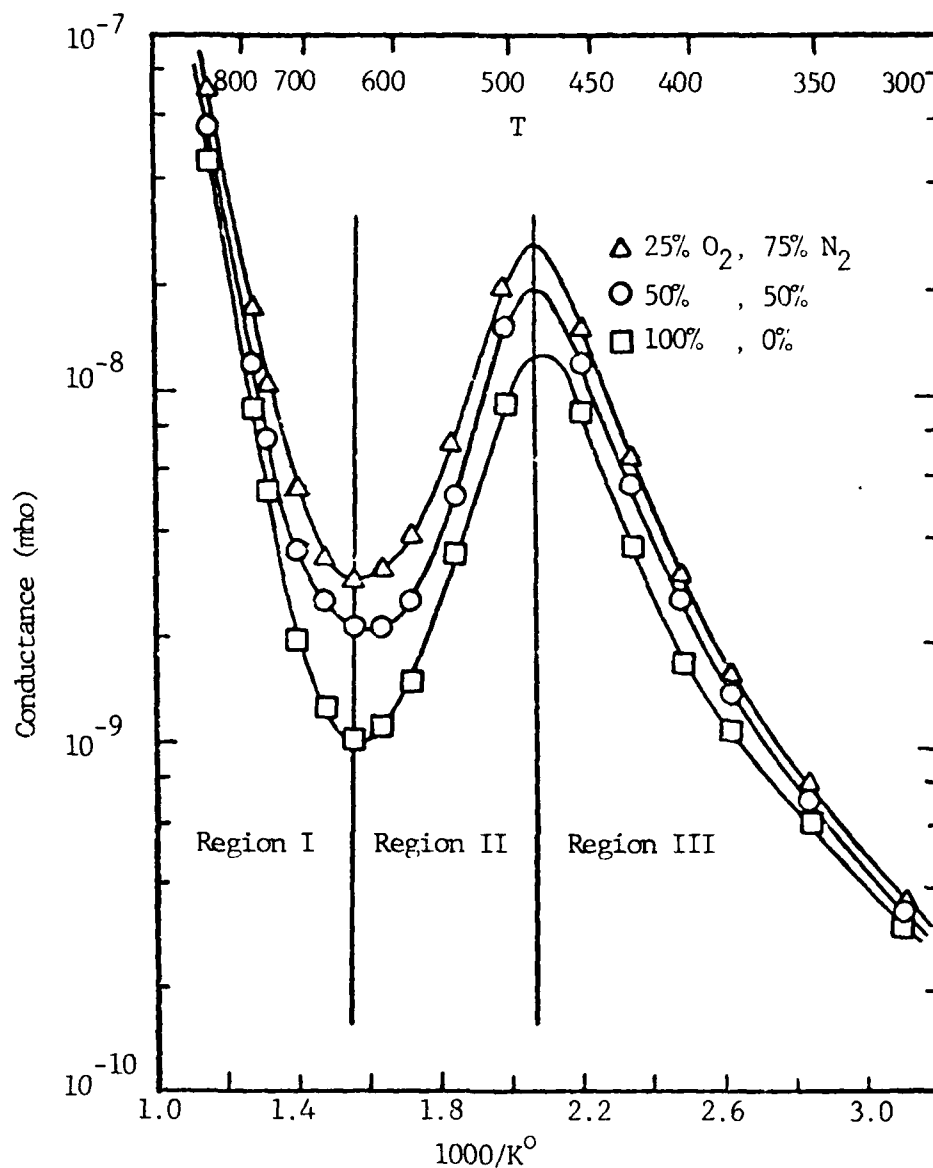


Figure 15. Electrical conductance of zinc oxide vs. increasing temperature for various partial pressures of oxygen.

of doped zinc oxide films was very poor compared to that of zinc oxide films. Advani (56) also reported response characteristics of tin oxide to oxygen. He mainly investigated the  $SnO_2$  film as a sensor for  $H_2S$  and  $H_2$ .

Wortman (50) used the RF sputtering method to fabricate zinc oxide films of various thicknesses on ceramic (pyrocera) substrate. The sensor construction is sketched in Figure 18, and Figures 19 and 20 show the characteristics of the  $ZnO$  film.

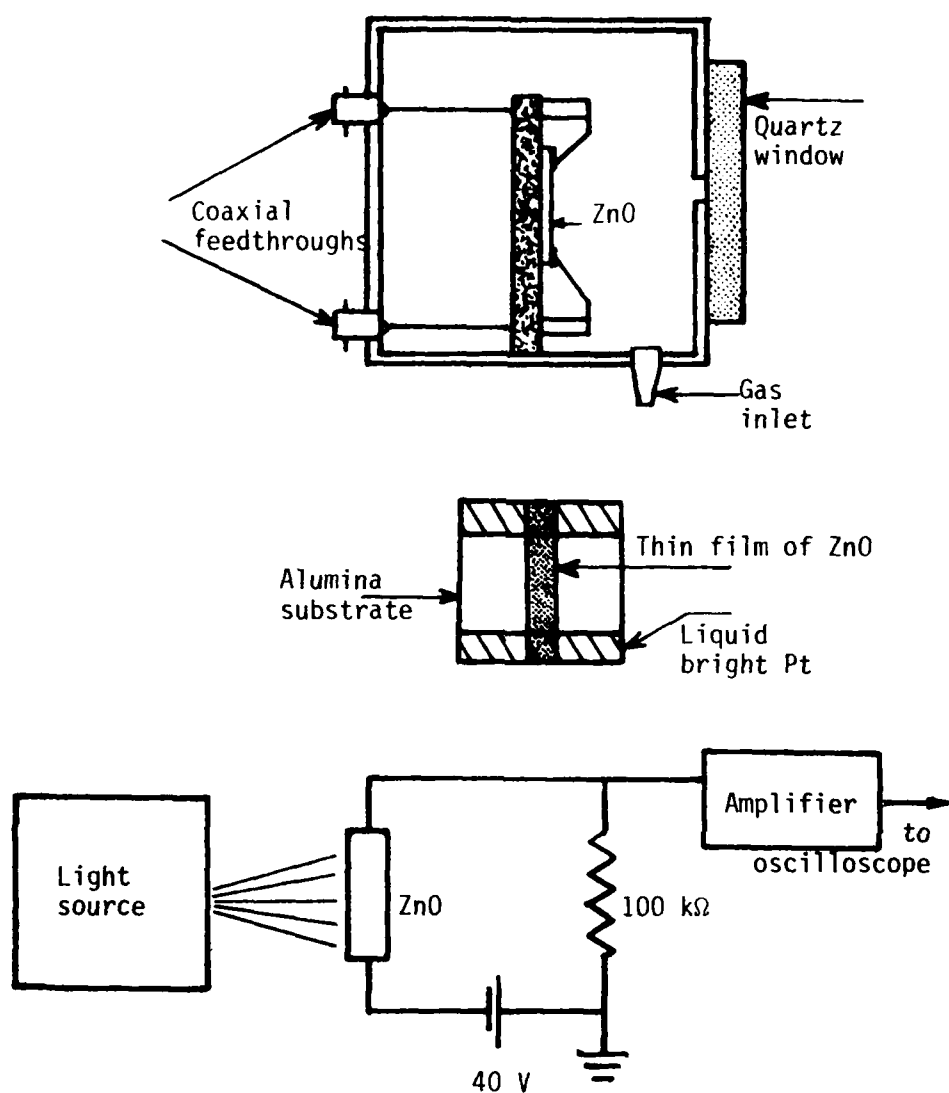


Figure 16. Photoconductivity sample holder and circuit arrangement for measuring photoresponse of ZnO in nitrogen and oxygen environments.

Figure 19 shows the change of the film resistance as a function of reciprocal temperature for three thicknesses of the ZnO film: the thickest film exhibits the lowest resistance. Wortman (50) noted, however, that the film resistance is also affected by sputtering conditions such as power level and gas pressure. Experimentally one can obtain the value of activation energy,  $E_a$ , (see Eq. 13) by taking the slope of the line in the region where the film resistance is linear. Some values of  $E_a$  for different gases are listed in Table 4 (50).

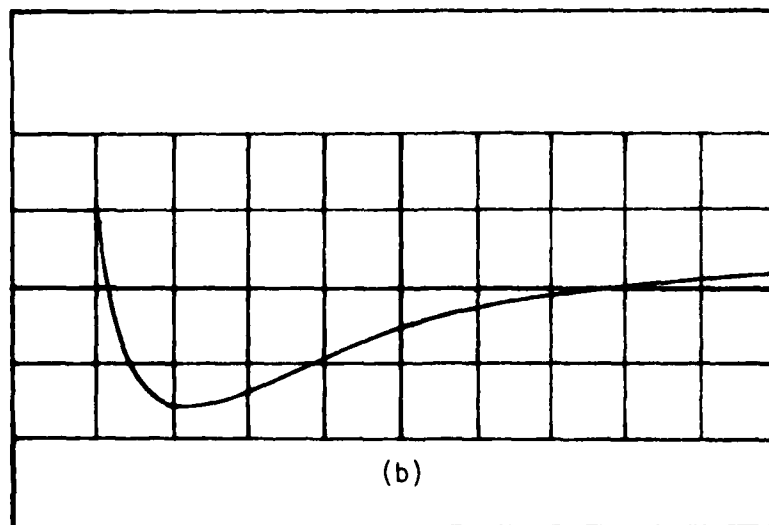
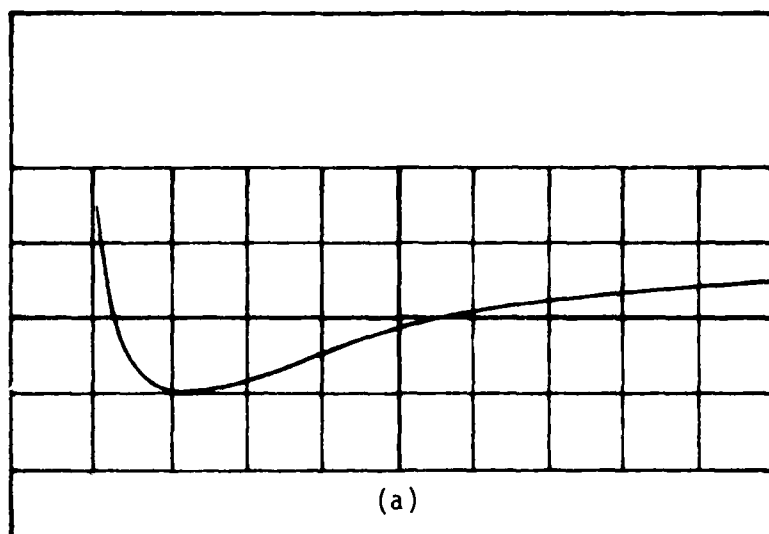


Figure 17. Typical photoconductivity response of ZnO in oxygen (a) and nitrogen (b) environments. Horizontal-20  $\mu\text{s}/\text{div.}$ , vertical-0.2  $\mu\text{A}/\text{div.}$ , base line-0.5 div. from the top grid line.

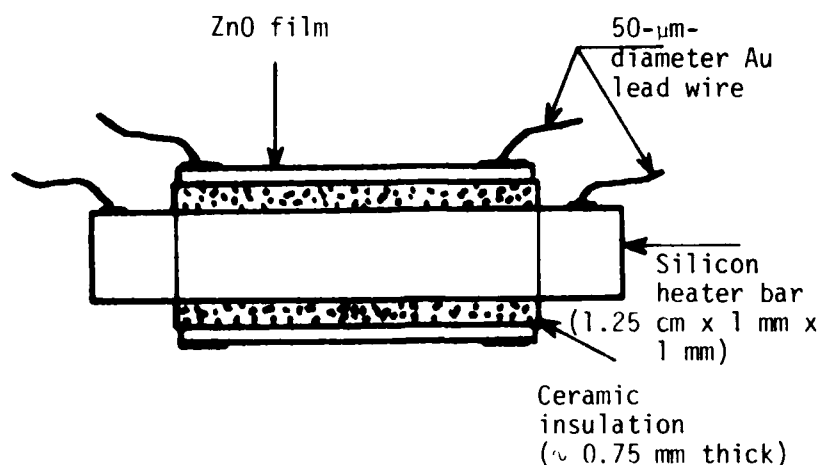


Figure 18. Cross-sectional view of Wortman's sensor.

TABLE 4. DEPENDENCE OF THERMAL ACTIVATION ENERGY ON TYPE OF GAS AND PRESSURE FOR 180-nm FILM

Pressure in $\text{N/m}^2$	Activation energy ( $E_a$ ) in eV		
	Ar	$\text{N}_2$	$\text{O}_2$
13.3	0.155	0.124	0.254
133	0.112	0.094	0.310

The selective response of ZnO film to oxygen gas is clearly demonstrated in Figure 20. The levels of the film resistance in Ar or  $\text{N}_2$  do not change significantly, whereas in  $\text{O}_2$  the resistance change is by a factor of about 6 at 573°K to about 15 at room temperature. It will be noted later, however, that at a lower-than-room temperature the sensor response becomes slow. Data given in Table 4 were obtained from Figure 20. As shown here and emphasized in Eq. 12, the value of  $E_a$  plays an important role in sensor characteristics.

The temperature effect on the sensor response is shown in Figure 21 (49). Note that Figure 21 only shows 50% response time; generally, for a full response, more than twice that time is needed (50).

**Summary**--Characteristics of a semiconductor thin-film oxygen sensor, ZnO, are reviewed. In contrast to stabilized zirconia sensors, the zinc oxide film sensor does not require the atmospheric pressure as a reference (see Eq. 13). As with the zirconia sensor, the higher the temperature, the faster the response. If the method of photoconductivity is used to measure oxygen partial pressure, the sensor can be operated at room temperature, and this method is quite promising because of its fast response.

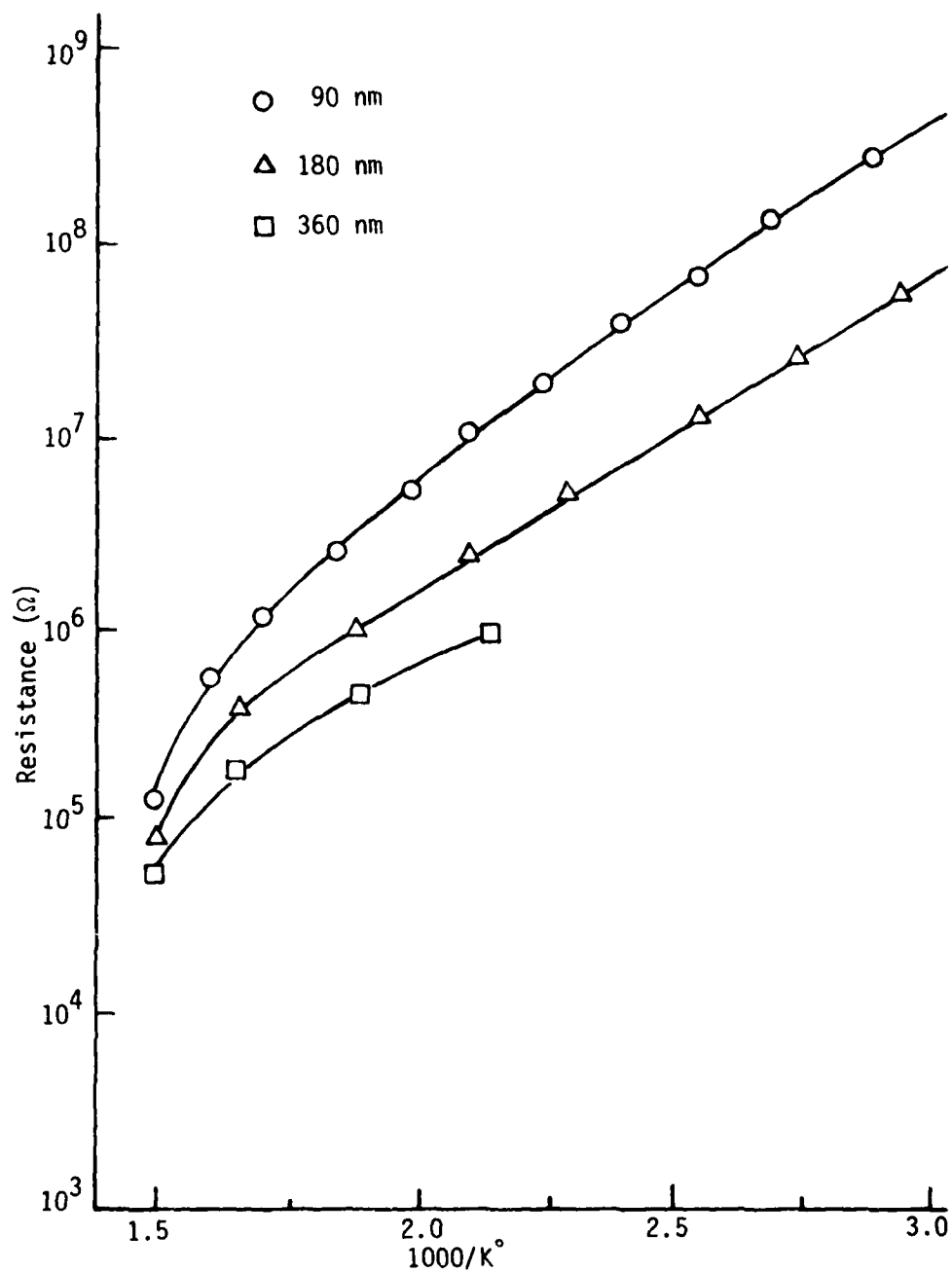


Figure 19. Resistance as a function of reciprocal temperature for three ZnO film thicknesses. Data taken at a constant cooling rate under 133 N/m<sup>2</sup> (1 Torr) oxygen pressure.



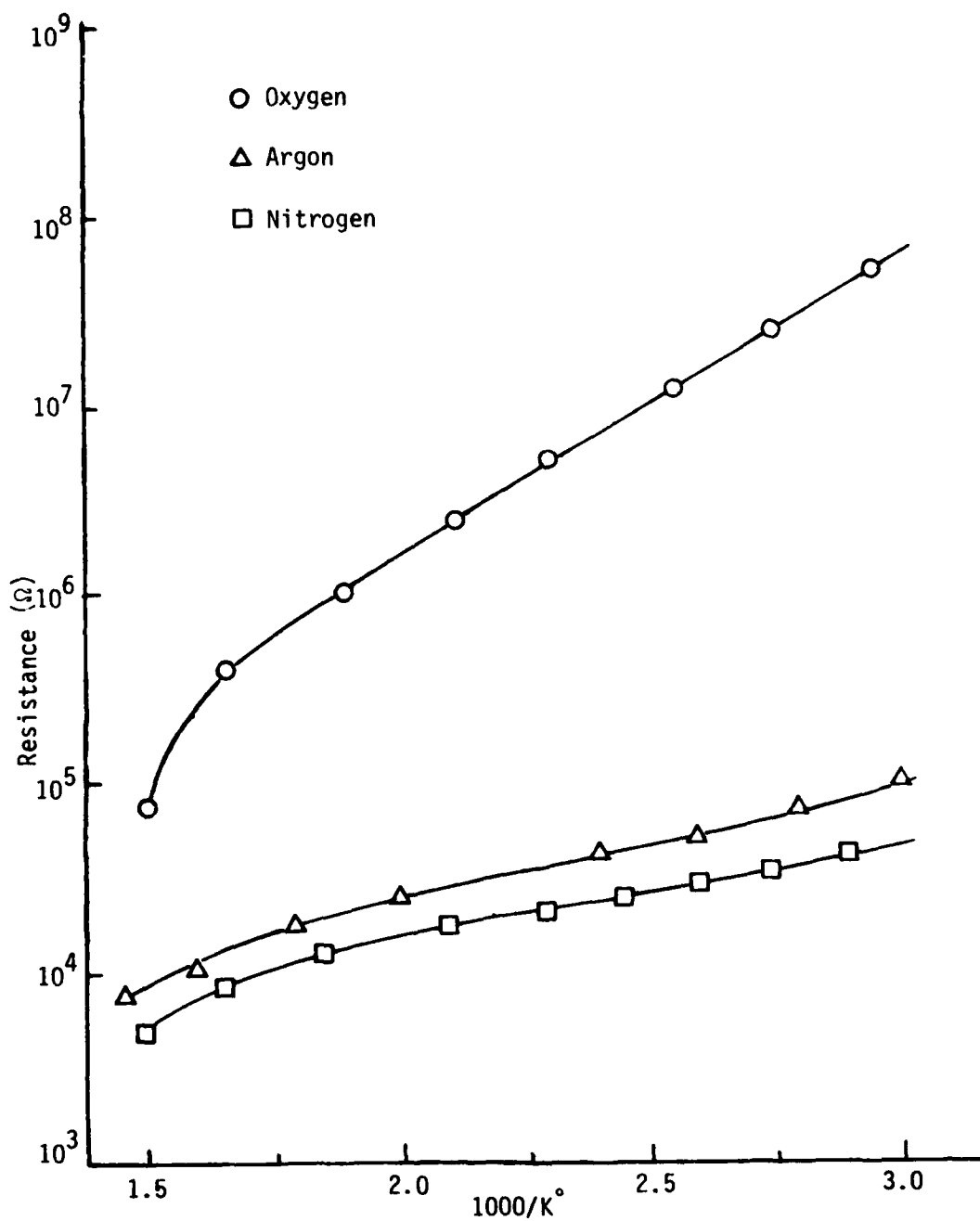


Figure 20. Resistance as a function of reciprocal temperature for 180-nm ZnO film at a constant cooling rate at a pressure of 133 N/m<sup>2</sup> (1 Torr) of the gases indicated.

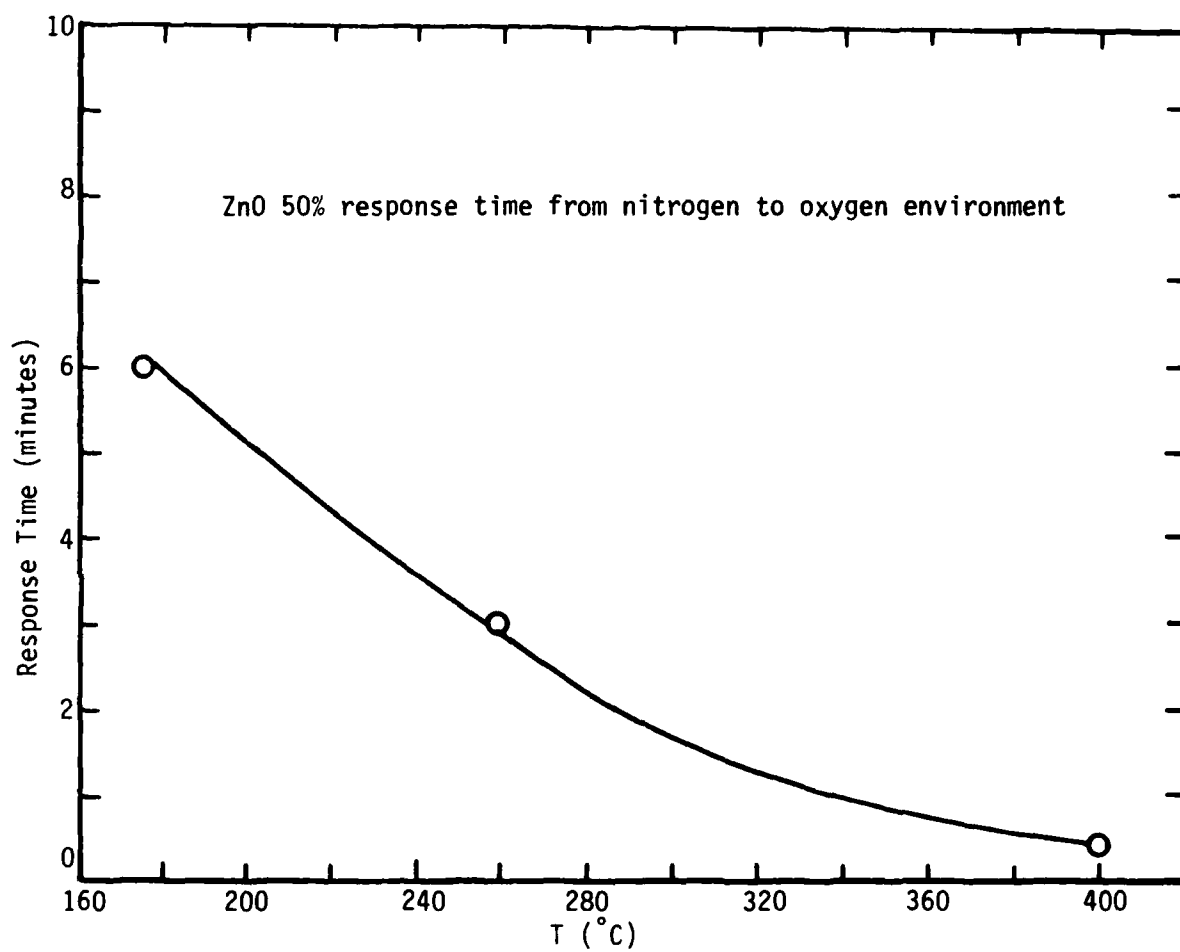


Figure 21. Response time vs. temperature.

## Rutile (Titanium Dioxide) Semiconductor

Titanium forms a number of oxides, such as  $Ti_2O$ ,  $Ti_3O_2$ ,  $TiO$ ,  $Ti_2O_3$ ,  $Ti_3O_5$ ,  $Ti_{n+2}O_{n+1}$  ( $n = 4-10$ ),  $Ti_{2n+2}O_{n+1}$  ( $n = 2-10$ ), and  $TiO_2$  (57, 58)<sup>7</sup>. Among them, strong reduction of  $TiO_2$  produces an n-type, blue-black, semiconductor which has an activation energy of 0.07 eV at room temperature and an intrinsic energy band gap of 3.12 eV (59, 60)<sup>8</sup>.

The reduced rutile semiconductor differs from elemental semiconductors in several respects. Probably the most important one is its high dielectric constant which ranges from 89 to 173, depending upon its preparation, crystal direction, and temperature. Another important distinction is the high melting point of 1840°C, which increases the difficulty of obtaining specimens of high purity (62). A related effect is the high concentration of oxygen vacancies that are "frozen" into the specimen at elevated temperatures. Oxygen vacancies are believed to exceed the cation vacancies in rutile. The formation of an oxygen vacancy in the otherwise pure oxide provides a source of two electrons having an activation energy less than the energy required to raise an electron to the conduction band in the stoichiometric material. Thus, it is believed that the presence of oxygen vacancies results in the nonstoichiometric rutile  $TiO_2$  (62)<sup>9</sup>.

The crystal structure of rutile is shown in Figure 22, where the tetragonal unit cell contains two  $TiO_2$  molecules. The structure is composed of a body-centered titanium sublattice: pairs of  $O^{2-}$  ions are placed between subsequent  $Ti^{4+}$  ions in alternating face-diagonal directions normal to the c-axis.

Nonstoichiometric rutile is classified as an n-type semiconductor on the basis of experimental observations (63-67): as with  $ZnO$ , the conduction is mostly "electronic" due to the defect structure of rutile<sup>10</sup>. The electronic conductivity of rutile in oxygen environment can be expressed by

---

<sup>7</sup> $Ti_2O_3$  is a p-type semiconductor at room temperature (61). Hurlen (57) and von Hippel et al. (58) have very good discussions on structure of rutile.

<sup>8</sup>The term "reduction" is used here to signify that an attempt has been made to introduce oxygen vacancies by heating the specimen in oxygen at reduced pressure (62).

<sup>9</sup>Grant (62) published a very comprehensive review article in 1959 which discusses almost every important property of rutile.

<sup>10</sup>Defects or imperfections in crystal lattices can be classified as reversible (ions in interstitial positions and ion vacancies connected with an equivalent number of quasi-free electrons and holes) or irreversible (flaws, cracks, dislocations). The present discussion is confined to the former class of defects.

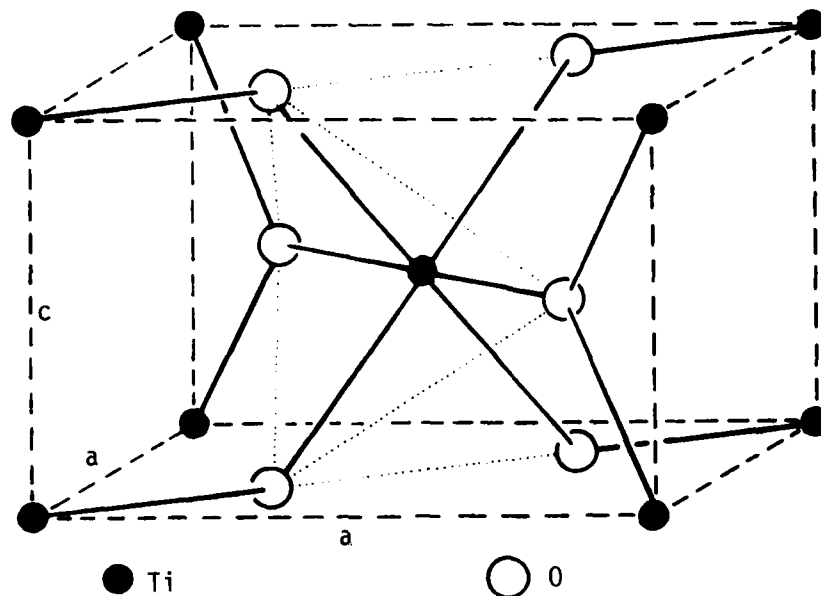
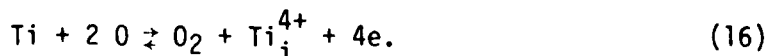
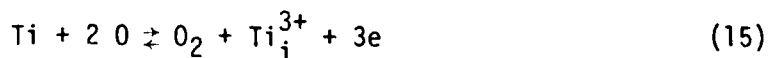


Figure 22. Unit cell of rutile ( $\text{TiO}_2$ ).

$$\sigma = K(T)p_{\text{O}_2}^{-1/\bar{n}} \quad (14)$$

where  $K(T)$  is a physical factor as a function of temperature (58), and  $\bar{n}$  ranging from 4 to 6 is determined theoretically or experimentally (57, 65) depending upon the type of defect (interstitial) reaction, such as



If one assumes either reaction (Eq. 15 or 16),  $\bar{n}$  can be uniquely determined. Many review papers have been written to argue about which reaction is taking place when  $\text{TiO}_2$  is exposed in oxygen environment (57, 58, 62, 63). Because slight experimental error can give false indication about the type of reaction taking place (64), Blumenthal (65) rationalized the reactions of nonstoichiometric rutile on the basis of a titanium interstitial model involving both triply and quadruply ionized titanium interstitials. His theoretical derivation for the electronic conductivity  $\sigma$  is, concisely, as follows:

A charge neutrality expression can result from Eqs. 15 and 16:

$$n = 3(\text{Ti}_i^{3+}) + 4(\text{Ti}_i^{4+}) + D \quad (17)$$

where  $n$  is the density of conduction electrons, and  $D$  is the concentration of ionized impurities that act as donors.

From the mass action equations for defect equilibria, one can obtain expressions which relate the concentration of ionized titanium interstitials to the concentration of conduction electrons and the partial pressure of oxygen

$$(\text{Ti}_i^{3+}) = C_3 p_{\text{O}_2}^{-1} n^{-3} \quad (18)$$

$$(\text{Ti}_i^{4+}) = C_4 p_{\text{O}_2}^{-1} n^{-4} \quad (19)$$

where  $C_3$  and  $C_4$  are the equilibrium reaction constants.

Substitution of Eqs. 18 and 19 into Eq. 7 yields

$$n = (3C_3 n^{-3} + 4C_4 n^{-4}) p_{\text{O}_2}^{-1} + D \quad (20)$$

which relates the concentration of conduction electrons to the partial pressure of oxygen.

For extrinsic electronic conduction

$$\sigma = ne\mu \quad (21)$$

where  $e$  is the electronic charge, and  $\mu$  is its mobility<sup>11</sup>.

The combination of Eqs. 20 and 21 yields a conductivity expression as a function of oxygen pressure:

$$\sigma^5 = (A\sigma + B) p_{\text{O}_2}^{-1} + D'\sigma^4 \quad (22)$$

where  $A = 3C_3 C_5^4$ ,  $C_5 = e\mu$ , and  $B = 4C_4 C_5^5$ .

Blumenthal (65) did similar analysis for a defect structure involving both singly and doubly ionized oxygen vacancies and ionized impurities that act as donor centers. However, he found the excellent agreement between Eq. 22 and the experimental data. This indicates that the conduction by ionized titanium interstitials is dominant<sup>12</sup>.

<sup>11</sup>Blumenthal also discussed intrinsic conduction in Ref. 66.

<sup>12</sup>Blumenthal (65) gives an extensive table for values of  $A$ ,  $B$ , and  $D'$  for titanium interstitials and oxygen vacancies.

Application--As with stabilized zirconia sensors, rutile  $\text{TiO}_2$  has not been widely applied as an oxygen sensor. Only the automobile industry has been experimenting with  $\text{TiO}_2$  as an exhaust-gas sensor (3, 15, 30, 68). Like the zirconia sensor, a rutile oxygen sensor senses the large change in the oxygen partial pressure at the stoichiometric A/F ratio (see Fig. 5). However, the  $\text{TiO}_2$  sensor does not require a reference pressure, which was necessary with zirconia sensors. Typical resistivity of  $\text{TiO}_2$  ceramic (as a function of partial oxygen pressure) is shown in Figure 23. The resistivity data generally follow the previously discussed theoretical curves (68).

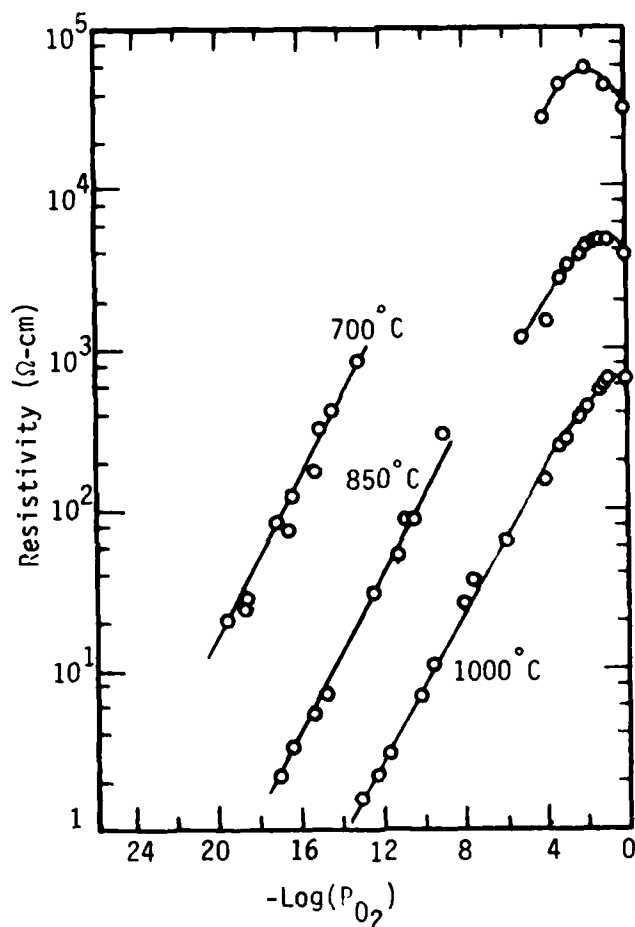


Figure 23. Resistivity of  $\text{TiO}_2$  ceramic as a function of partial oxygen pressure at several different temperatures.

A very simple oxygen sensor structure used by Tien (15) is shown in Figure 24. Response time of this type of sensor ranges from 0.2 to 0.5 s for 10-90% response. Gibbons (68) suggested that the  $\text{TiO}_2$  ceramic sensors should be operated at a temperature above 1000°C for simple interpretation of data.

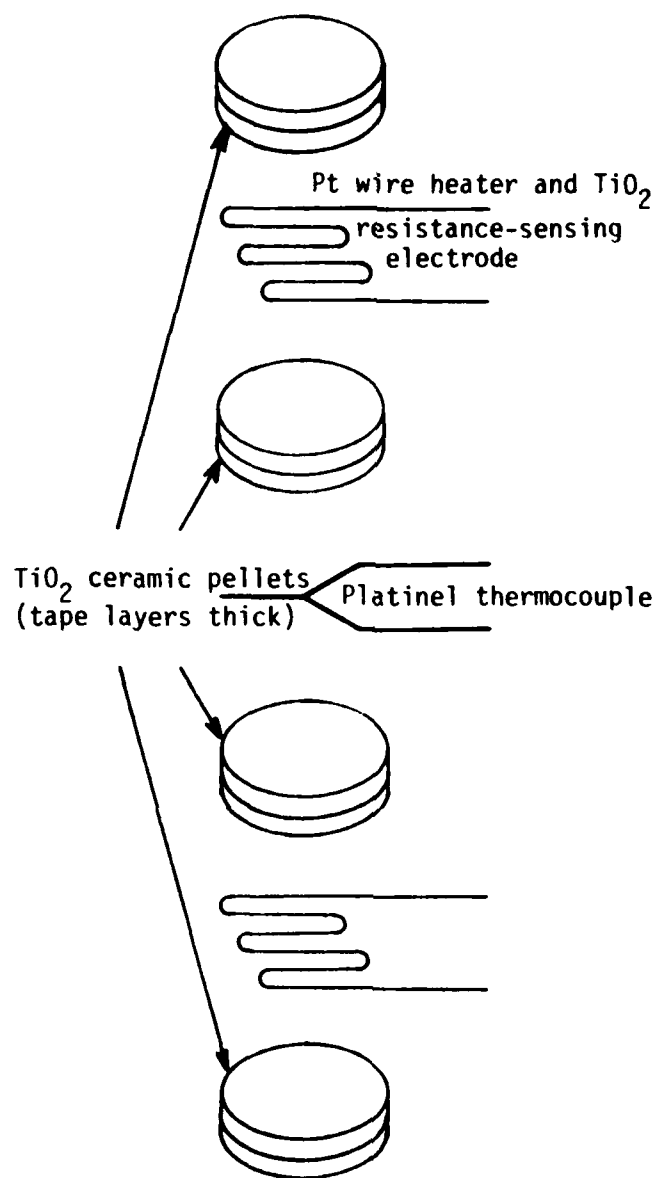


Figure 24. Exploded view of construction of temperature-stabilized  $\text{TiO}_2$  A/F sensor.

**Summary**--The rutile  $\text{TiO}_2$  ceramic is an n-type semiconductor. Unlike stabilized  $\text{ZrO}_2$  sensors, it does not require the atmospheric pressure as a reference for automobile application. At this point, the  $\text{TiO}_2$  sensor does not have distinctive advantages or disadvantages over  $\text{ZnO}$  semiconductor sensors, except its disadvantage of relatively high operating temperature ( $1000^\circ\text{C}$ ). It will be worthwhile to study the characteristics of  $\text{TiO}_2$  ceramic as an oxygen sensor for in-flight application.

### Other Oxygen Gas Sensors

Recently there have been many reports about ion-sensitive MIS (metal-insulator-semiconductor) (69) or MOS (metal-oxide-semiconductor) devices, with special interest on the structure which includes capacitors (70-74), diodes (75-78), and transistors (79-88). These devices are mainly designed to detect hydrogen and are known to work well with catalytic metals such as Pd and Pt on the oxide material. Lundström (81) has published a very good review paper.

The basic principles of hydrogen-sensitive Pd (or Pt)-Si-SiO<sub>2</sub> structure (Fig. 25) are explained as follows. Hydrogen molecules in the ambient are dissociated on the catalytic metal surface, and the atoms are adsorbed on the metal surface. Some of the hydrogen atoms diffuse through the thin metal film and are adsorbed on the metal-insulator interface. The number of adsorbed hydrogen atoms on the surface depends not only on the hydrogen pressure in the ambient but also on the other gases in the ambient. For example, in the presence of oxygen, chemical reactions take place on the metal surface. Hydrogen is taken away from the metal surface much more effectively by these reactions than by the fundamental backreaction  $2H \rightarrow H_2$ . Therefore, the number of hydrogen atoms at the interface, at a given hydrogen partial pressure, decreases (79).

Hydrogen atoms adsorbed at the interface (and on the surface) are "polarized" and give rise to a dipole layer. The dipole layer at the interface corresponds to a voltage drop,  $\Delta V$ , which is added to the externally applied voltage,  $V_G$  or  $V$ . The characteristics of the MOS structure are therefore shifted along the voltage axis by  $\Delta V$  volts (79). Söderberg (70) used the Kelvin probe (89) to observe similar effects by measuring the change in the work function due to the dipole layer.

Yamamoto (75) used Pd and TiO<sub>2</sub> (which is typically used as an oxygen-sensor ceramic) to design a hydrogen-sensitive device (Fig. 26). This device was also sensitive to oxygen pressure. Yamamoto's experimental sensor responses are shown in Figure 27 for  $p_{O_2} \approx 0$  and  $p_{O_2} = 1 \times 10^{-1}$  Torr; however, he reports that the responses were not reversible. ZnO, another oxygen-sensitive semiconductor, was investigated by Ito (76) with a Pd electrode to detect hydrogen gas. He reported that the Schottky barrier (Pd-ZnO) diode can be operated at room temperature.

Summary--When certain oxides are used with catalytic metals such as Pd or Pt, the change in the work function of the metal affects the characteristics of hydrogen-sensing devices. The change occurs more quickly than with the typical oxygen-sensing materials (TiO<sub>2</sub>, ZnO, and ZrO<sub>2</sub>). A typical response time of the Pd-oxide system is less than 2 minutes (76, 86-87). Stibler (85) reported 1-s response time of a hydrogen leak detector which was operated at 150°C.

All of the recently developed Pd-gate MOS transistors or Schottky diodes are designed primarily to detect hydrogen gas, not oxygen. One can hardly collect enough data on oxygen responses of such devices. Traditional oxygen-sensing materials, such as ZrO<sub>2</sub>, ZnO, and TiO<sub>2</sub>, are used with catalytic metals;



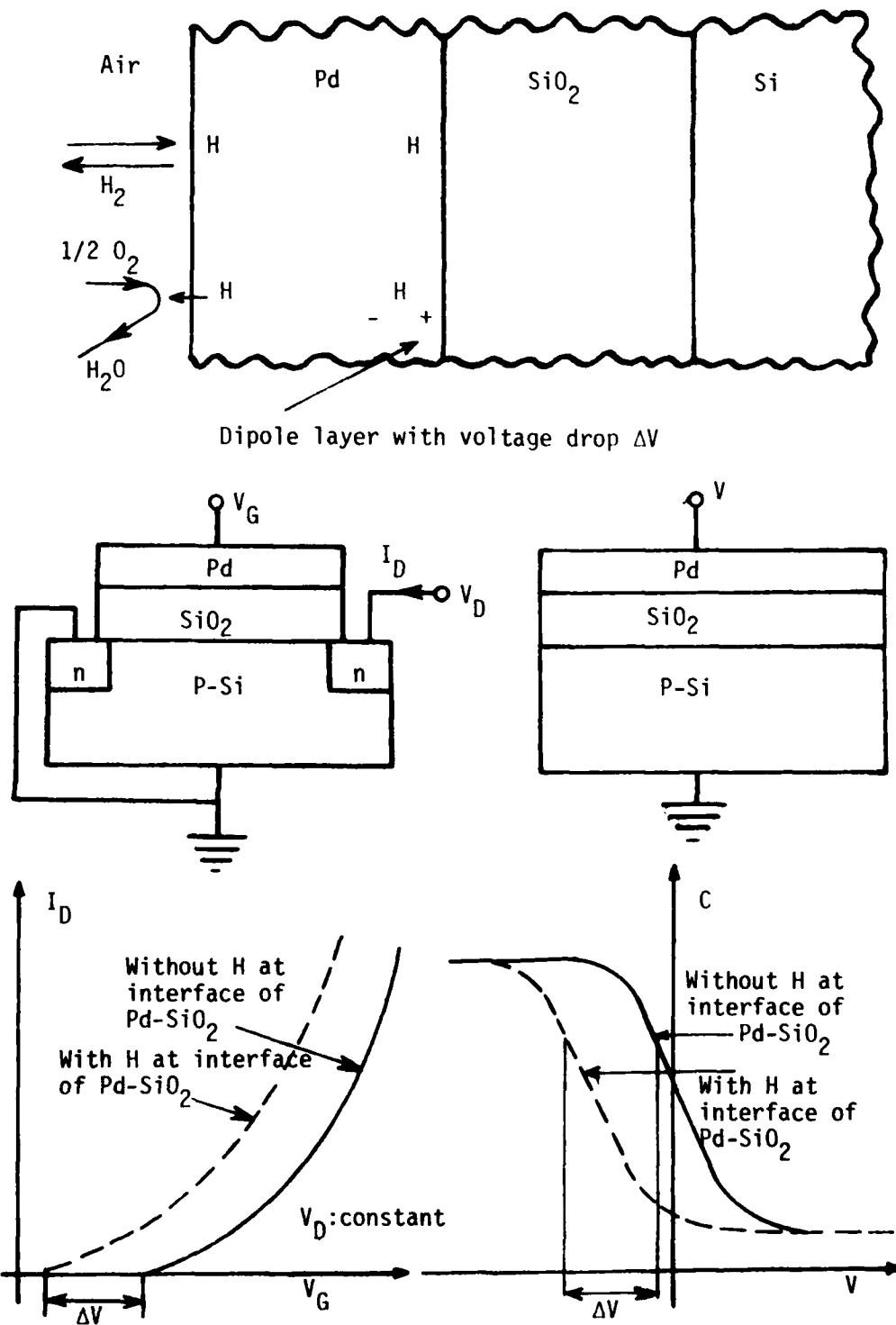


Figure 25. Basic principles of hydrogen-sensitive Pd (or Pt)- $SiO_2$ -Si structures.

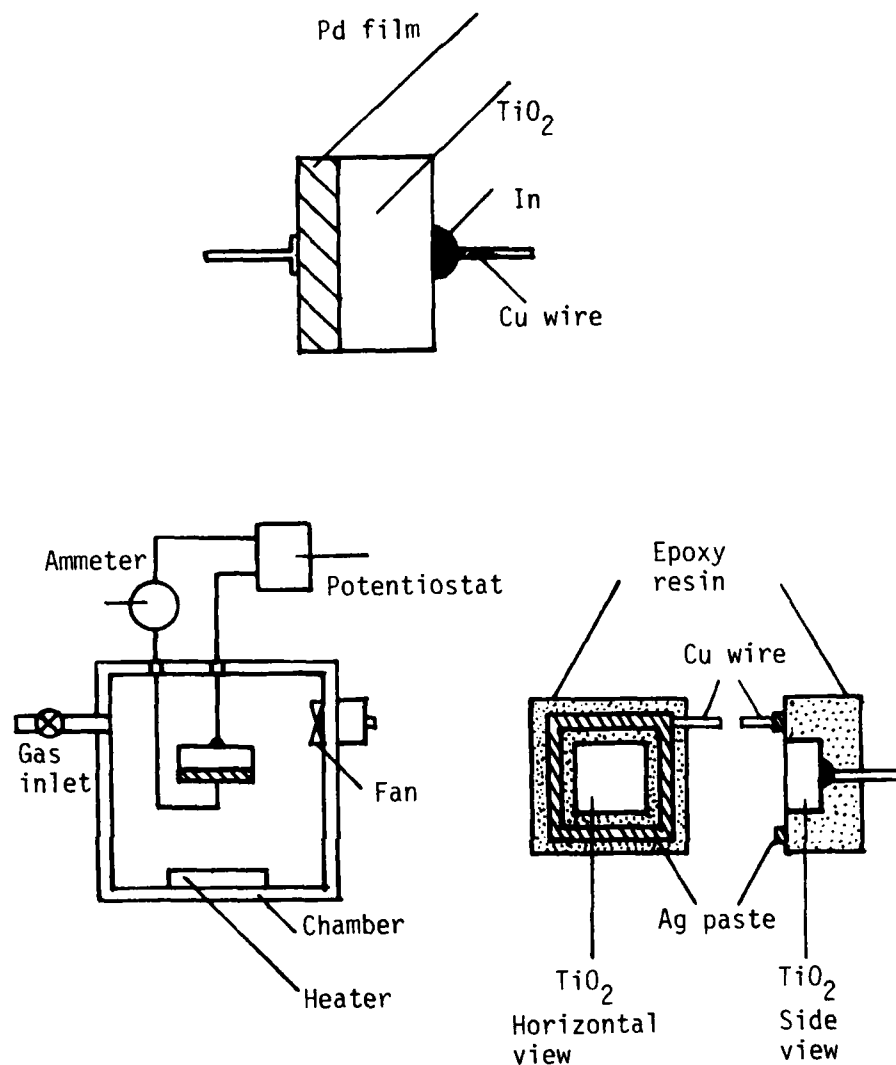


Figure 26. A schematic diagram of the Pd-TiO<sub>2</sub> diode and the measuring cell.

however, the main difference between the two systems lies in their detection schemes. The recently developed system utilizes the change in the gate voltage or the change in the work function of the catalytic metal due to the formation of dipole layers, while the traditional system uses the change in the electromotive force for electrolytes and the change in electric conductivity for semiconductors.

#### REVIEW AND RECOMMENDATIONS

In this report, the three most widely known oxygen-sensing materials--stabilized ZrO<sub>2</sub>, ZnO, and TiO<sub>2</sub>--are comparatively reviewed. The report also

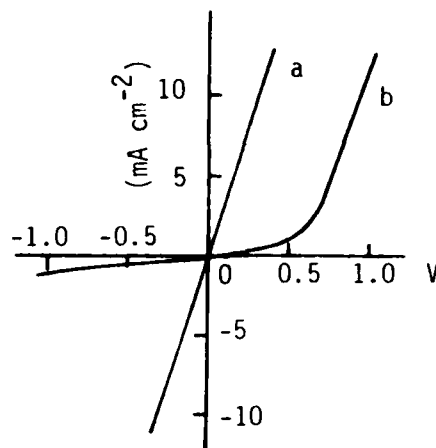


Figure 27. The I-V curves of a Pd-TiO<sub>2</sub> diode in vacuum ( $2 \times 10^{-5}$  Torr) (a), and in oxygen atmosphere ( $1 \times 10^{-1}$  Torr) (b).

contains a brief description of gas-sensing MOS transistors and diodes that use Pd or Pt as a catalytic electrode material.

The stabilized ZrO<sub>2</sub> is a solid-electrolyte ceramic material which develops an electromotive force across the opposite surfaces of the ceramic when it is exposed to an oxygen environment. This type of sensor requires use of a reference pressure for oxygen sensing, which would not be practical for in-flight application. It also needs to be heated at a temperature above 400°C. The conductivity of the zirconia is purely ionic.

ZnO is an n-type semiconductor whose band gap is 3.2 eV. When a ZnO film is in oxygen ambient, the film's conductivity decreases as the oxygen molecules get adsorbed on the surface. By observing the decrease in conductivity, one can measure the oxygen partial pressure. ZnO has been the most thoroughly investigated oxygen-sensing material, and its selective response to oxygen is well known. Unlike ZrO<sub>2</sub>, a ZnO sensor does not require a reference pressure for its operation.

The rutile TiO<sub>2</sub> ceramic is also an n-type semiconductor with an energy band gap of 3.12 eV. Like ZnO, the conduction of TiO<sub>2</sub> ceramic is mostly "electronic" due to the defect structure of rutile. At this point, TiO<sub>2</sub> does not seem to have any distinctive advantages or disadvantages over ZnO sensors, except the disadvantage of the relatively high typical operating temperature of 1000°C. The automobile industry is actively experimenting with TiO<sub>2</sub> along with stabilized ZrO<sub>2</sub>.

The type of sensors mentioned above use the bulk effect of the material as a sensing signal. Recently, however, a surface effect has been utilized to detect hydrogen gas with Pd-gate transistors or Pd-Schottky diodes. This

new method senses the dipole layers formed in the Pd metal film ( $\sim 1000 \text{ \AA}$ ) or senses change in the work function of the metal. This scheme gives a sensor response time on the order of a magnitude shorter than that of the ceramic sensors. The sensors of this kind have been investigated very little in an oxygen environment.

None of the sensors described were designed for in-flight use; moreover, no extensive experimental data on any kind of solid-state oxygen sensors is available for oxygen pressures ranging from  $5 \times 10^4$  to  $10^5$  Pascal (which is 0.5 to 1 atm). However, the solid-state sensor does offer the best promise for immediate improvement by fabrication and testing. Research efforts should initially be concentrated on eliminating the calibration problems and speeding up the sensor response time to the order of 1 or 2 s.

The calibration problem can be eliminated by strictly standardizing the fabrication process or post-treatment such as laser-beam trimming. For a shorter response time, one can use the time derivative of the conductivity signal of semiconductor sensors. With today's microprocessor technology, this kind of signal processing would be simple.

At this time, it is difficult to single out an oxygen sensor for the U.S. Air Force because insufficient practical experimental data exists. This study has shown, however, that it would be in the best interest of the Air Force to fabricate ZnO and TiO<sub>2</sub> sensors for testing. At the same time, the Air Force should conduct research to better understand the effect of catalytic metals, such as Pd or Pt, on MOS transistors or Schottky diodes. The result of the latter research can be immediately applied to the fabrication of electronic sensors with ZnO or TiO<sub>2</sub>.

## REFERENCES

1. Fitzmaurice, J. A. Survey of methods for the determination of oxygen in oxygen-enriched air. NBS Report 3130, Jan 1954.
2. IEEE transactions on electron devices. ED-26 (1979).
3. Esper, M. J., et al. Titania exhaust gas sensor for automotive applications. Presented at the International Automotive Engineering Congress and Exposition, Detroit, Mich., 1979.
4. Hamann, E., et al. Lambda-sensor with  $Y_2O_3$ -stabilized  $ZrO_2$ -ceramic for application in automotive emission control systems. Presented at the International Automotive Engineering Congress and Exposition, Detroit, Mich., 1977.
5. Croset, M., et al. Study of calcia-stabilized zirconia thin-film sensors. J Vac Sci Technol 14:777-781 (1977).
6. Fleming, W. J. Physical principles governing nonideal behavior of the zirconia oxygen sensor. Electrochem Sci Technol 124:21-28 (1977).
7. Fleming, W. J. Device model of the zirconia oxygen sensor. Presented at the International Automotive Engineering Congress and Exposition, Detroit, Mich., 1977.
8. Young, C. T., et al. Characteristics of  $ZrO_2$ -type oxygen sensors for automotive applications. Presented at the International Automotive Engineering Congress and Exposition, Detroit, Mich., 1979.
9. Göpel, W. Reactions of oxygen with  $ZnO$ - $10\bar{1}0$ -surfaces. J Vac Sci Technol 15:1298-1310 (1978).
10. Lagowski, E. S., et al. Quantitative study of the charge transfer in chemisorption; oxygen chemisorption on  $ZnO$ . J Appl Phys 48:3566-3575 (1977).
11. Göpel, W. Oxygen interaction of stoichiometric and nonstoichiometric  $ZnO$  prismatic surfaces. Surface Sci 62:165-182 (1977).
12. Many, A. Relation between physical and chemical processes on semiconductor surfaces. CRC Crit Rev Solid State Sci 4:515-539 (1974).
13. Arizs, E., et al. The influence of surface donor states on the chemisorption kinetics of oxygen at the surface of  $ZnO$  single crystals. J Solid State Chem 6:310-318 (1973).
14. Tench, A. J., et al. Oxygen species adsorbed on zinc oxide. Chem Phys Lett 8:177-178 (1971).

15. Tien, T. Y., et al.  $\text{TiO}_2$  as an air-to-fuel ratio sensor for automobile exhausts. *Ceram Bull* 54:280-285 (1975).
16. Rickert, H. General aspects of solid electrolytes, sec. A, pp. 3-17. In W. van Gool (ed.). *Fast ion transport in solids*. New York: American Elsevier Publishing Co., Inc., 1973.
17. Farrington, G. C. Solid ionic conductors. Presented at the NATO Advanced Study Institute on Chemically Sensitive Electronic Devices, Hightstown, N.J., 1980.
18. Eddy, D. S. Physical principles of the zirconia exhaust gas sensor. *IEEE Transactions on Vehicular Technology*. VT-23:125-128 (1974).
19. Kingery, W. D., et al. Oxygen ion mobility in cubic  $\text{Zr}_{0.85}\text{Ca}_{0.15}\text{O}_{1.85}$ . *J Am Ceram Soc* 42:393-398 (1959).
20. Tien, T. Y., et al. X-ray and electrical conductivity of the fluorite phase in the system  $\text{ZrO}_2\text{-CaO}$ . *J Chem Phys* 39:1041-1047 (1963).
21. Hund, F. The fluoritphase in system  $\text{ZrO}_2\text{-CaO}$ ; its defect structure and electrical conductivity. *Z Physik Chem* 199:142-151 (1952).
22. Kiukkola, K., et al. Measurements on galvanic cells involving solid electrolytes. *J Electrochem Soc* 104:379-387 (1957).
23. Dueker, H., et al. Ceramic aspects of the Bosch Lambda-sensor. Presented at the Automotive Engineering Congress and Exposition, Detroit, Mich., 1975.
24. Strickler, D. W., et al. Electrical conductivity in the  $\text{ZrO}_2$ -rich region of several  $\text{M}_2\text{O}_3\text{-ZrO}_2$  systems. *J Am Ceram Soc* 48:286-289 (1965).
25. Strickler, D. W., et al. Sonic conductivity of cubic solid solutions in the system  $\text{CaO-Y}_2\text{O}_3\text{-ZrO}_2$ . *J Am Ceram Soc* 47:122-127 (1964).
26. Weissbart, J., et al. Oxygen gauge. *Rev Sci Inst* 32:593-595 (1961).
27. Fouletier, J., et al. Electrochemical semipermeability and the electrode microsystem in solid oxide electrolyte cells. *Electrochem Sci Technol* 123:204-213 (1976).
28. Croset, M., et al. Study of calcia-stabilized zirconia thin-film sensors. *J Vac Sci Technol* 14:777-781 (1977).
29. Gopal, E. S. R. Statistical mechanics and properties of matter: theory and applications, ch. 13. New York: John Wiley & Sons, 1976.
30. Glasstone, S. Thermodynamics for chemists, ch. 12, pp. 250-272. New York: Nostrand Co, Inc., 1947.

31. Emission control of engine systems. Consultant report to the committee on motor vehicle emissions, commission on sociotechnical systems, National Research Council, Sept 1974.
32. Ichikawa, N., et al. Oxygen sensor. U.S. patent 4,164,462, Aug 1979.
33. Cederquist, A. L., et al. Characterization of zirconia and titania engine exhaust gas sensors for air/fuel feedback control systems. Presented at the Automotive Engineering Congress and Exposition, Detroit, Mich., 1976.
34. Fleming, W. J. Temperature sensitivity mapping of the zirconia oxygen sensor: engine test results. Presented at the Automotive Engineering Congress and Exposition, Detroit, Mich., 1976.
35. Fleming, W. J., et al. Sensor for on-vehicle detection of engine exhaust gas composition. Presented at the Automotive Engineering Meeting, Detroit, Mich., 1973.
36. D'Allea, B. A., et al. Relation of exhaust gas composition to air-fuel ratio. Presented at the Annual Meeting of the Society of Automobile Engineers, Detroit, Mich., 1936.
37. Dixon, J. M., et al. Electrical resistivity of stabilized zirconia at elevated temperatures. J Electrochem Soc 110:276-280 (1963).
38. Heiland, G., et al. Electronic processes in zinc oxide, vol. 8, pp. 191-323. In F. Seitz and D. Turnbull (eds.). Solid state physics. New York: Academic Press, 1959.
39. Gmelins handbuch der organischen chemie, 8th ed., zink, ergänzungsband. Verlag chemie, Weinheim/Bergstrasse, Germany, 1956.
40. Göpel, W. Reactions of oxygen with ZnO-10 $\bar{1}$ 0-surface. J Vac Sci Technol 15:1298-1310 (1978).
41. Lagowski, J., et al. Quantitative study of the charge transfer in chemisorption; oxygen chemisorption on ZnO. J Appl Phys 48:3566-3575 (1977).
42. Morrison, S. R. The chemical physics of surface. New York: Plenum Press, 1977.
43. Tompkins, F. C. Chemisorption of gases on metals. New York: Academic Press, 1978.
44. Adamson, A. W. Physical chemistry of surfaces, 3rd ed. New York: John Wiley & Sons, 1976.
45. Flood, E. A. (ed) The solid-gas interface, vols. 1 and 2. New York: Marcel Dekker, Inc., 1967.
46. Many, A. Relation between physical and chemical processes on semiconductor surfaces. CRC Crit Rev Solid State Sci 4:515-539 (1974).

47. Garcia-Moliner, F. The band picture in the electronic theories of chemisorption on semiconductors. *Catal Rev* 2:1-66 (1968).
48. Vol'kenshtein, F. F. The electronic theory of catalysis on semiconductors. Oxford: Pergamon Press, 1963.
49. Royal, T. M., et al. An investigation of thin oxygen partial pressure sensors. NASA CR-1182 (1968).
50. Wortman, J. J., et al. Thin film oxygen partial pressure sensor. NASA CR-1941 (1972).
51. Shapira, Y., et al. Chemisorption, photodesorption and conductivity measurements on ZnO surfaces. *Surf Sci* 54:43-59 (1976).
52. Van Hove, H., and Luyckx, A. Photoconductivity decay of ZnO crystals in oxygen. *Solid State Commun* 4:603-606 (1966).
53. Collins, R. J., and Thomas, D. G. Photoconduction and surface effects with zinc oxide crystals. *Phys Rev* 112:388-395 (1958).
54. Medved, D. B. Photodesorption in zinc oxide semiconductor. *J Chem Phys* 28:870-873 (1957).
55. Matthews, H. E., and Kohnke, E. E. A preliminary study of certain electrical properties of stannic oxide ceramics. NASA CR-376 (1966).
56. Advani, C. N., and Jordan, A. G. Thin films of SnO<sub>2</sub> as solid state gas sensors. *J Electron Mater* 9:29-49 (1980).
57. Hurlen, T. On the defect structure on rutile. *Acta Chem Scand* 13:365-376 (1959).
58. von Hippel, A., et al. Protons, dipole, and charge carriers in rutile. *J Phys Chem Solids*, 23:779-799 (1962).
59. Cronmeyer, D. C. Electrical and optical properties of rutile single crystals. *Phys Rev* 87:876-886 (1952).
60. Frederikse, H. P. R. Recent studies on rutile (TiO<sub>2</sub>). *J Appl Phys* 32:2211-2215 (1961).
61. Pearson, A. D. Studies on the lower oxides of titanium. *J Phys Chem Solids* 5:316-327 (1958).
62. Grant, F. A. Properties of rutile (titanium dioxide). *Rev Mod Phys* 31:646-674 (1959).
63. Earle, M. D. The electrical conductivity of titanium dioxide. *Phys Rev* 61:56-63 (1942).



64. Tannhauser, D. S. Experimental evidence from conductivity measurements for interstitial titanium in reduced  $\text{TiO}_2$ . *Solid State Commun* 1:223-225 (1963).
65. Blumenthal, J. R. N., et al. Electrical conductivity of nonstoichiometric rutile single crystals from 1000°C to 1500°C. *J Phys Chem Solids* 27:643-654 (1966).
66. Blumenthal, J. R. N., et al. Studies of the defect structure of nonstoichiometric rutile  $\text{TiO}_{2-x}$ . *Solid State Sci* 114:172-176 (1967).
67. Blumenthal, J. R. N., et al. Electronic mobility in rutile ( $\text{TiO}_2$ ) at high temperatures. *J Phys Chem Solids* 28:1077-1079 (1967).
68. Gibbons, E. F., et al. Automotive exhaust sensors using titania ceramic. Presented at Automotive Engineering Congress and Exposition, Detroit, Mich., 1975.
69. Cheung, P. W. (ed.), et al. Theory, design, and biomedical applications of solid state chemical sensors. West Palm Beach, Florida: CRC Press, Inc., 1978.
70. Söderberg, D., et al. Catalytic reactions on metals studied by work function measurements. *Mater Sci Engr* 42:141-144 (1980).
71. Duš, R. Surface reactivity of hydrogen with oxygen on palladium and palladium hydride films. *J Catal* 42:334-343 (1976).
72. Lundström, I., and DiStefano, T. Influence of hydrogen on Pt-SiO<sub>2</sub>-Si structures. *Solid State Commun* 19:871-875 (1976).
73. Steele, M. C., et al. Hydrogen-sensitive palladium gate MOS capacitors. *J Appl Phys* 47:2537-2538 (1976).
74. Conrad, H., et al. Adsorption of hydrogen on palladium single crystal surfaces. *Surf Sci* 41:435-446 (1974).
75. Yamamoto, N., et al. A study on a palladium - titanium oxide Schottky diode as a detector for gaseous components. *Surf Sci* 92:400-406 (1980).
76. Ito, K. Hydrogen-sensitive Schottky barrier diodes. *Surf Sci* 86:345-352 (1979).
77. Steele, M. C., and MacIver, B. A. Palladium/cadmium-sulfide Schottky diodes for hydrogen detection. *Appl Phys Lett* 28:687-688 (1976).
78. Shivaraman, M. S., et al. Hydrogen sensitivity of palladium-thin-oxide-silicon Schottky barriers. *Electron Lett* 12:483-484 (1976).
79. Lundström, I. Hydrogen-sensitive MOS structure. Presented at the NATO Advanced Study Institute on Chemically Sensitive Electronic Devices, Hightstown, N.J., 1980.

80. Danielsson, B., et al. On a new enzyme transducer combination: the enzyme transistor. *Anal Lett* 12 (B11): 1189-1199 (1979).
81. Lundström, I., et al. Chemical reactions on palladium surfaces studied with Pd-MOS structures. *Surf Sci* 64:497-519 (1977).
82. Lundström, I., and DiStefano, T. Hydrogen-induced interfacial polarization at Pd-SiO<sub>2</sub> interfaces. *Surf Sci* 59:23-32 (1976).
83. Shivaraman, M. S. Detection of H<sub>2</sub>S with Pd-gate MOS field-effect transistors. *J Appl Phys* 47:3592-3593 (1976).
84. Lundström, I., et al. Hydrogen in smoke detected by the Pd-gate field-effect transistor. *Rev Sci Instrum* 47:738-740 (1976).
85. Stibler, L., and Svensson, C. Hydrogen leak detector using a Pd-gate MOS transistor. *Rev Sci Instrum* 46:1206-1208 (1975).
86. Lundström, I., et al. A hydrogen-sensitive MOS field-effect transistor. *Appl Phys Lett* 26:55-57 (1975).
87. Lundström, I., et al. A hydrogen-sensitive Pd-gate MOS transistor. *J Appl Phys* 46:3876-3881 (1975).
88. Zemel, J. N. Ion-sensitive field effect transistors and related devices. *Anal Chem* 47:255A-268A (1975).
89. Engelhardt, H. A., et al. An accurate and versatile vibrating capacitor for surface and adsorption studies. *J Phys [E]* 10:1133-1136 (1977).

ATE  
LMED  
-8